Institut für Geophysik und Meteorologie
Technische Universität Braunschweig

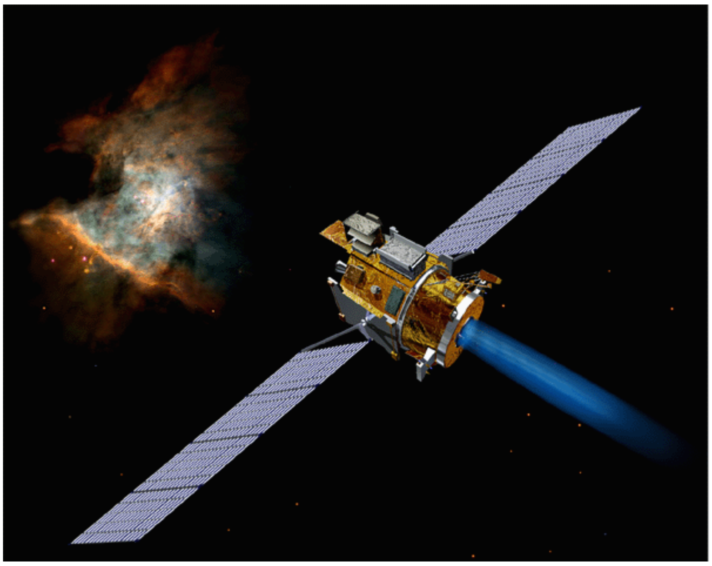

Abschlußbericht zum Vorhaben:

DS1 – New Millennium, Magnetometerexperiment, Kometenvorbeiflug, Ionentriebwerkdiagnose

Anschlußantrag zu Projekt: 50 OO 99037

Förderkennzeichen des DLR:	50 OO 0102
Bewilligungszeitraum:	01.06.2001 ... 31.12.2001
Berichterstatter:	Prof. Dr. K.-H. Glaßmeier
	Dr. G. Musmann
	Dr. I. Richter

Braunschweig, Juni 2002

Inhaltsverzeichnis

1 Beschreibung des Vorhabens

Deep Space 1 ist eine Satellitenmission der amerikanischen Weltraumbehörde NASA mit dem Ziel, 12 neuartige Technologien für die Raumfahrt des nächsten Jahrtausends zu testen. Als wesentliche Merkmale für dieses Projekt sind zu nennen:

- DS1 wird als erstes Raumfahrzeug auf einer Deep Space Mission mit einem Ionentriebwerk angetrieben.
- DS1 hat ein Experiment zur Plasmauntersuchung (PEPE – Plasma Experiment for Planetary Exploration) an Bord.
- DS1 ist mit zwei Fluxgatemagnetometern (FGM) ausgestattet. Sie wurden hier am Institut für Geophysik und Meteorologie in Braunschweig in Zusammenarbeit mit dem Institut für Datenverarbeitungsanlagen und dem Institut für Weltraumforschung in Graz, Österreich entwickelt und im institutseigenen Magnetlabor Magnetsrode kalibriert.

Neben der erfolgreichen Validierung der beschriebenen neuen Technologien standen als wissenschaftliche Zielsetzungen die beiden Vorbeiflüge am Asteroiden Braille im Juli 1999 und am Kometen Borrelly im September 2001 im Mittelpunkt dieser Mission. Diese Rendezvous sollten Erkenntnisse über Eigenschaften kleiner Himmelskörper und ihre Wechselwirkung mit dem Sonnenwind liefern.

Der erfolgreiche Flyby am Asteroiden Braille war Gegenstand des DS–1 Mutterprojektes (DLR-Förderkennzeichen: 50 OO99037) und wurde im dazugehörigen Abschlußbericht ausführlich analysiert. Hierzu wurde außerdem eine Veröffentlichung in den Geophysical Research Letters (GRL) verfaßt (s. Anlage B)

Hauptforschungsobjekt dieses Folgeprojektes ist nun der Flyby am Kometen Borrelly.

Es wird gezeigt, daß auch an Bord eines "magnetisch schmutzigen" Raumfahrzeug (DS–1 benötigt für den Ionenantrieb starke, bewegliche Focussiermagnete, die ein temperaturabhängiges Magnetisches Moment besitzen) wissenschaftlich signifikante Magnetfelddaten der durchquerten Zielregion gemessen werden können.

So wurden bereits im DS–1 Mutterprojekt Methoden entwickelt, die jetzt verfeinert wurden, um mit den beiden Braunschweiger Fluxgate–Magnetometer–Sensoren, die Plasmaumgebung des Kometen Borrelly zu charakterisieren. Mit diesem Werkzeug gelingt es, flugphasenspezifische Magnetfeldmodelle von DS–1 zu kreieren, die die wesentlichen Satellitenparameter zur Störfeldeliminierung enthalten und somit das gewünschte Feld des Kometen enthüllen.

Die entwickelten Methoden und die erhaltenen Daten wurden sowohl auf Postern (s. Anlage D), in einem Vortrag auf der Tagung der European Geophysical Society in Nizza 2001 (s. Folien in Anlage A), und in einem GRL–Paper (in Arbeit) der wissenschaftlichen Öffentlichkeit vorgestellt.

Parallel zur Auswertung der Magnetfelddaten wurde am Institut für Geophysik und Meteorologie eine numerische Simulation entwickelt, mit der die plasmaphysikalischen Phänomene in der Umgebung des Ionentriebwerks untersucht werden sollen. Bei dieser Simulation handelt es sich um einen drei-dimensionalen elektromagnetischen Teilchen-Code, der in Zusammenarbeit mit dem Rechenzentrum der TU Braunschweig auf dem dortigen Parallelrechner implementiert wurde. Angewendet wird der Code derzeit auf das sog. Neutralisationsregime – den sich dem Triebwerk unmittelbar anschließenden Raumbereich, in dem der Ionenstrahl durch injizierte Elektronen neutralisiert wird.

Auch hierzu wurde im Rahmen dieses Vorhaben eine weitere Veröffentlichung (s. Anlage C) in den Proceedings der International School for Space Plasma Simulations (ISSS) verfaßt.

En Detail lassen sich diese Ergebnisse in der Dissertation von Dr. Carsten Othmer (Numerical simulations of ion thruster-induced plasma dynamics, IGM, 2001) nachlesen.

2 Missionsablauf

DS1 wurde am 24. Oktober 1998 am Kennedy Space Flight Center, Cap Caneveral, erfolgreich gestartet. Nach dem spektakulären Braille Vorbeiflug in nur 28 km Entfernung im September 1999 wurde die urprünglich nur für 1 Jahr geplante Mission verlängert, da noch genügend Xenon–Treibstoff vorhanden war, um den Kometen Borrelly zu erreichen. Dieser Komet, der bislang noch von keinem Raumfahrzueg angeflogen wurde, stieß zum Zeitpunkt des Rendezvous in einer Sonnenentfernung von 1.34 AU von unten durch die Ekliptik, während sich DS–1 mit einer Relativgeschwindigkeit von 16.58 km/s in der Ekliptik näherte. Der Vorbeiflug fand in Bezug auf den Sonnenwind stromaufwärts in einer minimalen Entfernung von 2170 km unter einem Phasenwinkel von 93.7° statt.

Wärend des Vorbeifluges konnten etwa 6 Stunden lang vektorielle Magnetfelddaten mit einer Zeitauflösung von 1 s, und in unmittelbarer Nähe des Kometen 40 Minuten lang zeitlich hochaufgelöste (20 Hz) Daten gesammelt werden.

3 Das Fluxgate–Magnetometer

Die beiden Magnetometer für DS1 wurden am Institut für Geophysik und Meteorologie von Dr. F. Kuhnke unter der Leitung von Prof. K. H. Glaßmeier und Dr. G. Musmann entwickelt. Umfangreiche Funktionstests sowie die Kalibrierung der Magnetometer fanden im institutseigenen Magnetlabor „Magnetsrode“ statt. Siehe Abschlußbericht zum DS–1 Mutterprojekt.

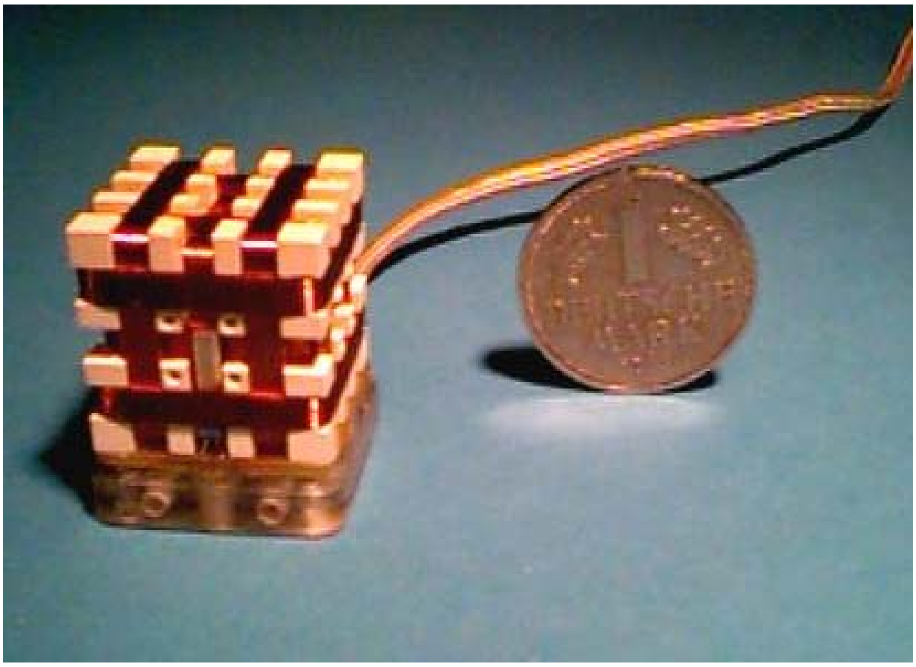

Abbildung 1: Der FGM–Sensor

Das Magnetometer besitzt eine Auflösung von 0.04 nT bei einem Meßbereich von 25000 nT. Es kann in einem Temperaturbereich von -150°C bis +300°C operieren und besticht durch eine extrem niedrige Leistungsaufnahme von etwa 200 mW. Die 3 Magnetfeldkomponenten können mit einer Sampling Rate von bis zu 20 Vektoren pro Sekunde gemessen werden.

DS–1 ist mit zwei solcher Magnetometer ausgestattet. Sie befinden sich außerhalb des Raumfahrzeuges auf dem 50 cm langen Magnetometerstummelboom.

4 Ergebnisse

4.1 Magnetfelduntersuchungen in Nähe des Kometen Borrelly

Während des FlyBys von DS–1 am Kometen Borrelly wurden sogennante Scandaten (1Hz) und hochaufgelöste (20 Hz) Magnefelddaten gemessen. Diese Daten wurden einem umfangreichen Preprocessing unterzogen:

- Einarbeitung der Kalibriermatrizen
- Koordinatentransformation auf gemeinsame Spacecraftkoordinaten
- Eliminierung der Spikes, die sekündlich von den Satellitensteuerdüsen erzeugt wurden. Die Steuerdüsen waren aktiv, um die gewünschte Trajektorie und Orientierung des Raumfahrzeugs um den Kometen herum zu ermöglichen, damit er im FoV der Kameras lag.
- Berücksichtigung des Temperaturmodells der Ionenstrahlfocussiermagnete. Eliminierung aller Temperatureinflüsse.
- Trennung der magnetischen Einflüsse des Satelliten (unterschiedlich auf beiden Magnetometern) und der Wirkung des externen Magnetfeldes (gleich auf beiden Magnetometern) durch Anwendung der Principal Component Analysis (PCA).
- Einarbeitung der s/c Attitude und der Positionsdaten, um das Magnetfeld in BSE–Koordinaten (Borrelly centered solar ecliptic) darstellen zu können.

Mit den so vorbehandelten Daten wurden folgende wissenschfaftliche Fragestellungen untersucht:

- Flyby Geometrie (s. Folie Anlage A)
- Darstellung aller Magnetfeldkomponenten während des Vorbeifluges.
- Untersuchung der Feld–Drapierung um den Kometen herum (s. Folie, Anlage A).
- Bestimmung des Bow–Shocks.
- Untersuchung einer etwaigen magnetischen Cavity-Region.
- Vergleich der Ergebnisse mit Daten anderer Kometen wie Halley, Giacobini–Zinner und Grigg-Skellerup.
- Spektrale Untersuchungen der Magnetfelddaten (verschiedene Spektren außerhalb und innerhalb des Bow Shocks, dynamisches Spektrum für den kompletten FlyBy). Siehe Folien, Anlage A.
- Gyrofrequenzanalyse zur Detektierung und Bestimmung vorhandener Ionenspecies.

Zu all diesen Punkten betrachte man die Folien des Vortrages auf der EGS–Konferenz (Anlage A).

4.1.1 Das Feld in Kometennähe – Auswertung der 1 Hz Daten

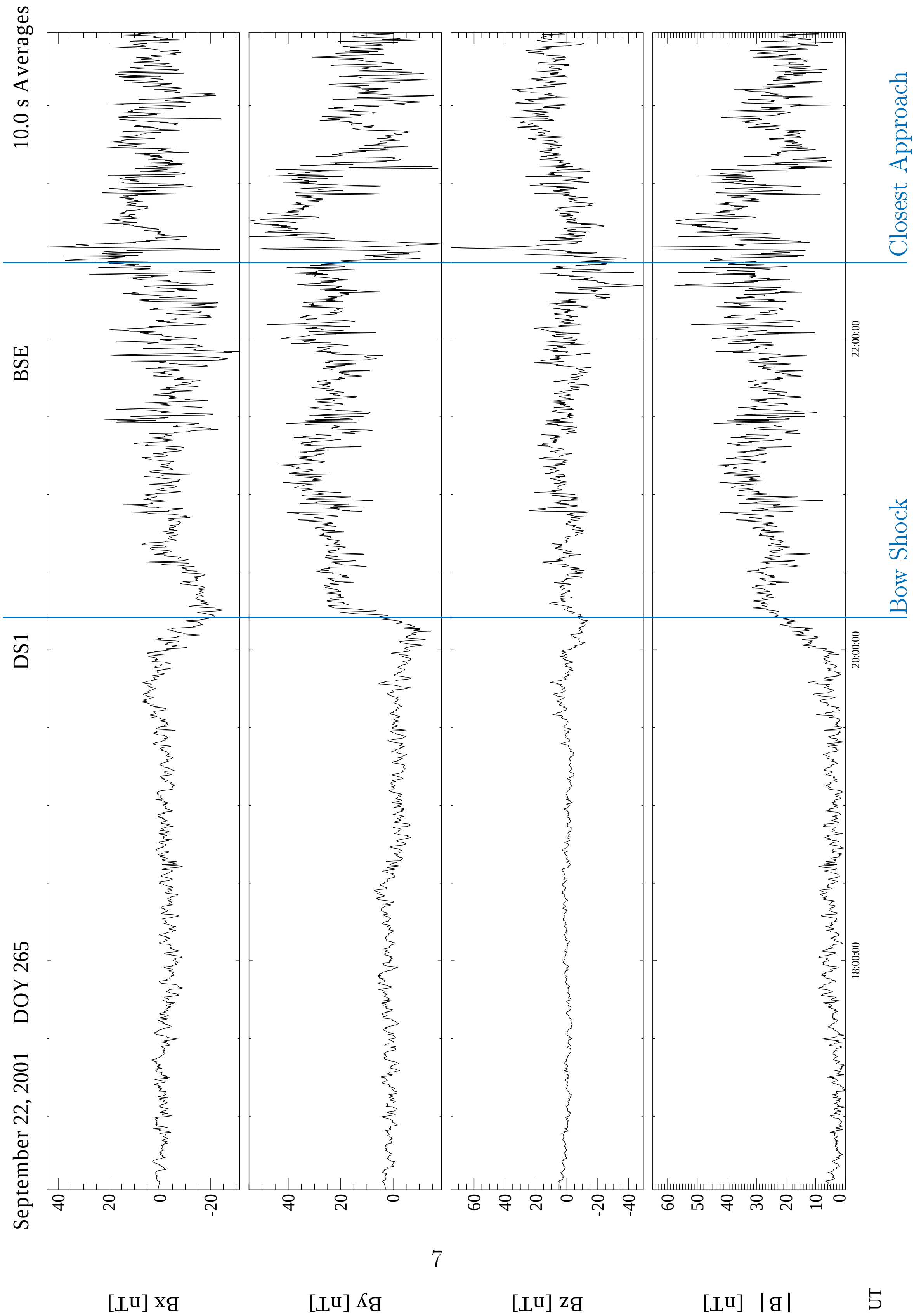

4.1.2 Das Feld direkt beim Closest Approach – Auswertung der 20 Hz Daten

In unmittelbarer Nähe des Closest Approach (C/A) sind für etwa 40 Minuten hochaufglöste (20 Hz) Magnetfeddaten verfügbar. Sie sind in der folgenden Graphik dargestellt. Das besondere hierbei ist, daß das Maximum im Magnetfeld erst etwa 5 Minuten nach dem C/A erscheint. Das Maximum der Ionendichte beim PEPE Experiment erscheint dagegen sogar etwa 4 Minuten früher, was jedoch auf die spezifische Schweif- und Jetstruktur des Kometen zurückzuführen ist;sie soll hier nicht näher beleuchtet werden.

Die Asymmetrie des Magnetfeldpeaks könnte mit einer ausgeprägten asymmetrischen Ringstromstruktur oder gar mit einer Eigenmagnetisierung des Kometen zusammenhängen. Dieses Phänomen wird zur Zeit noch untersucht.

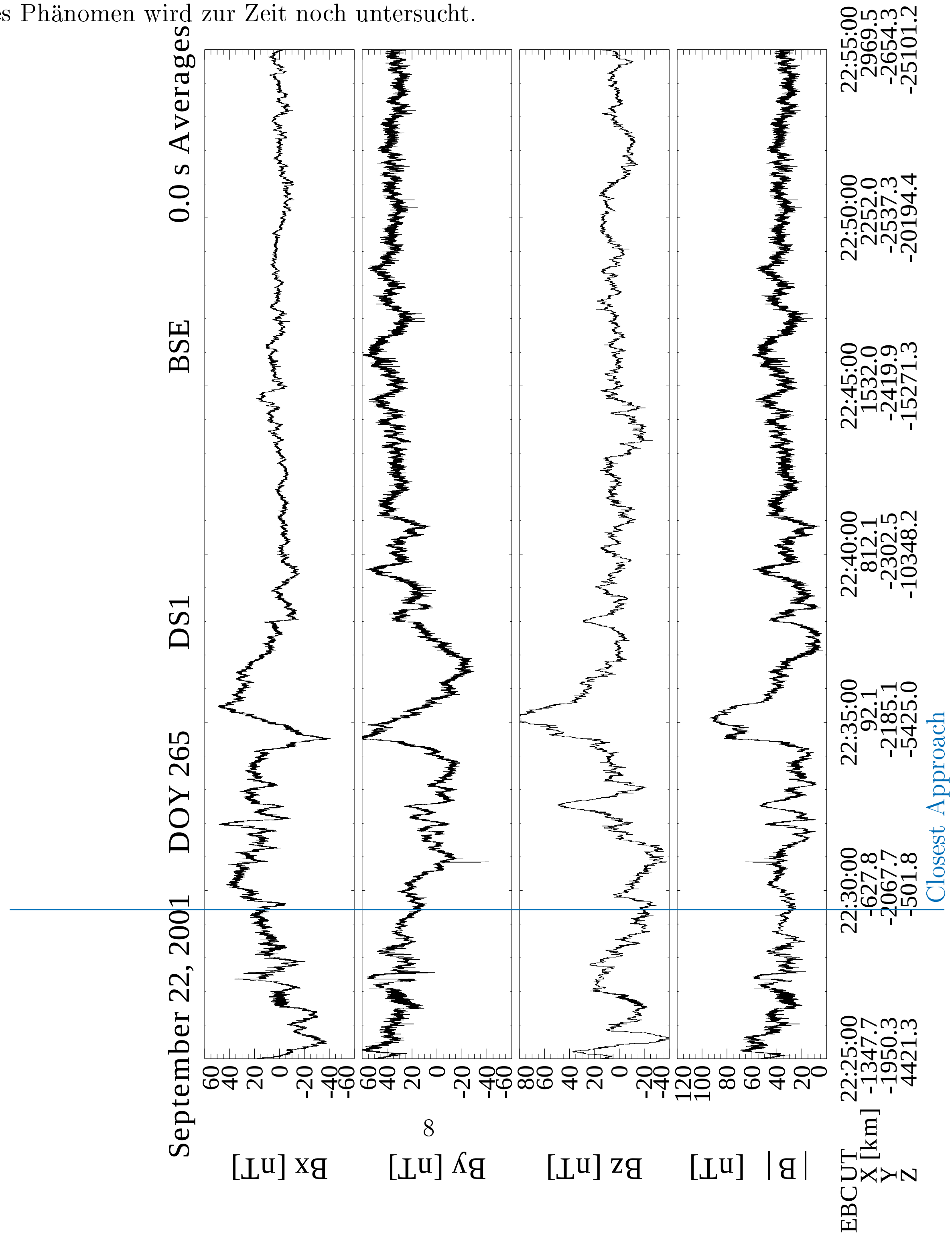

4.1.3 Bestimmung des Bow Shocks

Während des Vorbeifluges sendete DS–1 etwa 6 Stunden lang Magnetfelddaten zur Erde. Aufgrund von s/c Telemetriebeschränkungen konnte leider nicht mehr gemessen werden, so daß nur das inbound leg zur Bestimmung des Bow shocks zur Verfügung steht (s. Trajektorie in Anlage A). Die Bow Shock Distanz wurde zu R_{sub}= 93800 km bzw. $R_{\perp}$= 140700 km abgeschätzt. Dieses Ergebnis steht in sehr guter Übereinstimmung zu theoretisch ermittelten Werten anhand der Formeln von [Huddleston, 1990] und [Galeev,1985].

4.1.4 Untersuchung einer etwaigen magnetischen Cavity-Region

Die Ausdehnung der bei Kometen auftretenden Cavity-Region wurde aus dem Gleichgewicht zwischen auswärtsgerichtetem Ionen–Neutralteilchen Druck und der inwärtsgerichteten $\underline{j} \times \underline{B}$ Kraft abgeschätzt [Cravens 1986]. Als Ergebnis zeigt sich, daß eine Cavity erst in einer Kometen Entfernung von etwa 400 km zu erwarten ist; bei einer Flyby Entfernung von 2170 km ist daher kein magnetfeldfreier Raum zu beobachten.

4.1.5 Vergleich von Borrelly mit anderen Kometen

Die folgende Tabelle zeigt eine Übersicht über alle relevanten Parameter der 4 untersuchten Kometen. Die Daten wurden teils aus der einschlägigen Literatur zusammengetragen, teils neu berechnet (z.B. Bow Shock Entfernung, s. o.)

Die Graphik auf der übernächsten Seite zeigt die Magnetfeldbeträge, die bei den Vorbeiflügen an den Kometen Halley, Grigg-Skjellerup, Giacobini-Zinner und Borrelly gemessen wurden. Die Zeitachsen wurden gemäß der unterschiedlichen Vorbeiflugparameter gedehnt bzw. gestreckt, um die physikalisch bedeutungsvollen Strukturen optisch geeignet darstellen zu können. Die Ähnlichkeit zwischen den Kometen ist evident. Somit war der Vorbeiflug am Borrelly ein weiterer Meilenstein, der das aktuelle Verständnis um die Kometenphysik untermauert.

Giacobini-Zinner  Halley  Grigg-Skjellerup 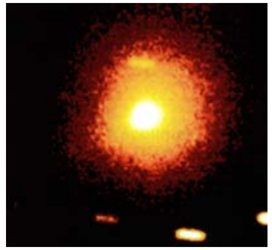 Borrelly 

Mission		ICE (11.09.85)	Giotto (13.03.86)	Giotto (10.07.92)	DS 1 (22.09.01)
Fly By Trajectory		Tail	Upstream	Tail	Upstream
CA distance	R_{ca} [km]	7862	596	200	2172
CA velocity	v_{ca} [km/s]	20.7	68.7	14.0	16.6
Heliocentric Distance	R_h [AU]	1.03	0.89	1.01	1.36
Phase Angle	α [deg]	83.6	107.2	89.3	93.7
Dimensions	l*w*h (Radius) [km^3]	(1)	16 x 7.5 x 8, (5.5)	(1.3)	8 x 4 x 4, (3)
Orbital Period	T [y]	6.52	76.10	5.09	6.86
SW mass	m_{sw} [mp]	1.15	1.15	1.15	1.15
SW velocity	v_{sw00} [km/s]	490	380	350	362
SW density	n_{sw00} [1/km^3]	5.10E+15	5.96E+15	9.14E+15	5.25E+15
SW mass density	ρ_{00} [kg/km^3]	9.81E-12	1.15E-11	1.76E-11	1.01E-11
SW flux	n_{sw00}*v_{sw00} [1/(km^2 s)]	2.50E+18	2.27E+18	3.20E+18	1.90E+18
Gas outflow velocity	v_e [km/s]	1	1	1	1
Gas production rate	Q [1/s]	3.00E+28	1.00E+30	3.60E+27	2.90E+28
Photoionisation Rate	ν_{ph} [1/s]	3.15E-07	4.22E-07	3.27E-07	1.81E-07
Charge exch.cross sect.	σ[km^2]	2.10E-25	2.10E-25	2.10E-25	2.10E-25
Total ionisation rate	ν [1/s]	8.40E-07	8.98E-07	9.99E-07	5.80E-07
Ionisation scale length	L [km]	1.19E+06	1.11E+06	1.00E+06	1.73E+06
Contact surface field calc.	B_{cs} [nT]	77	65	74	58
Contact surface Distance	R_{cs} [km]	317	5245	68	412
Flux @ Bow shock	n_B*v_B [1/(km^2 s)]	2.75E+18	2.65E+18	3.90E+18	2.09E+18
Critical flux ratio	$Flux_B/Flux_{00}$	1.1	1.17	1.22	1.1
Bow Shock Distance	R_{Sub} [km]	74000	769000	6600	93800
Perp. Bow Shock Distance	R_{perp} = 1.5 R_{Sub} [km]	111000	1153500	9900	140700

Magnetic Field Measurements during Comet Fly Bys

Giotto @ Halley
March 13, 1986

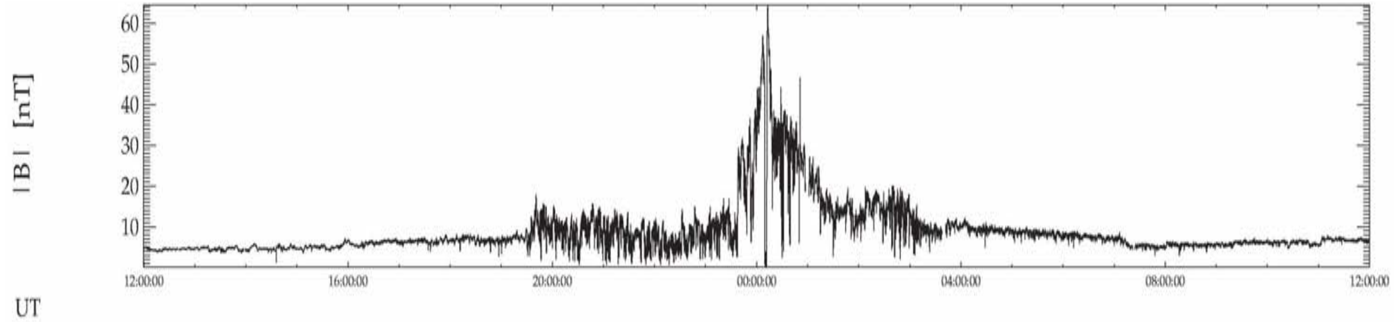

Giotto @ Grigg-Skjellerup
July 10, 1992

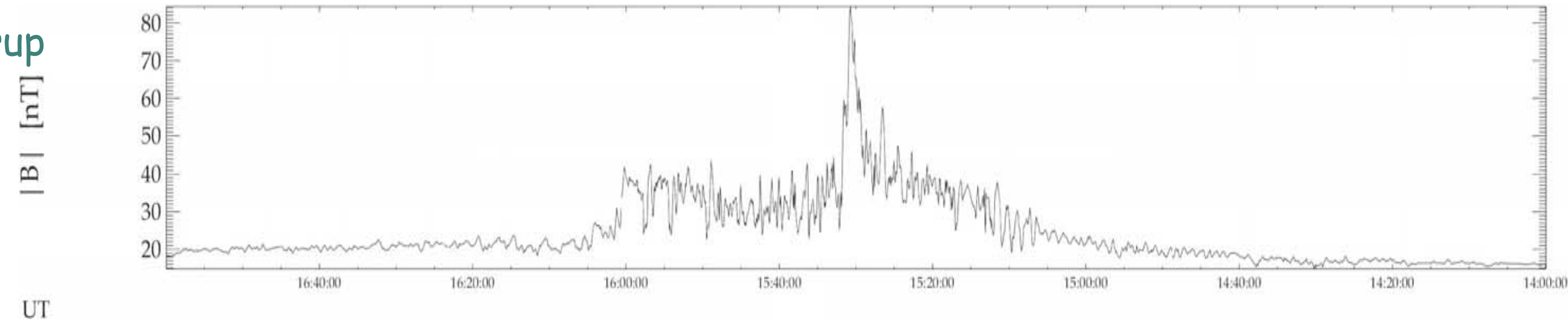

ICE @ Giacobini-Zinner
September 11, 1985

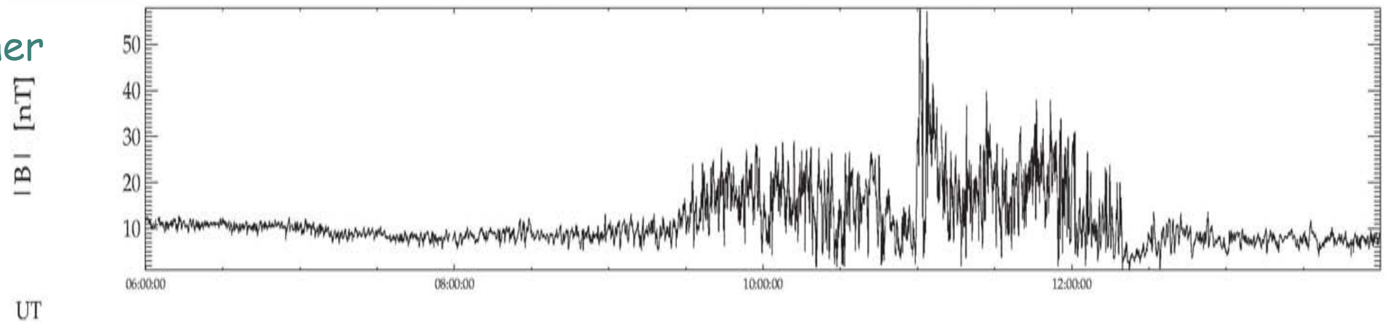

Deep Space 1 @ Borrelly
September 22, 2001

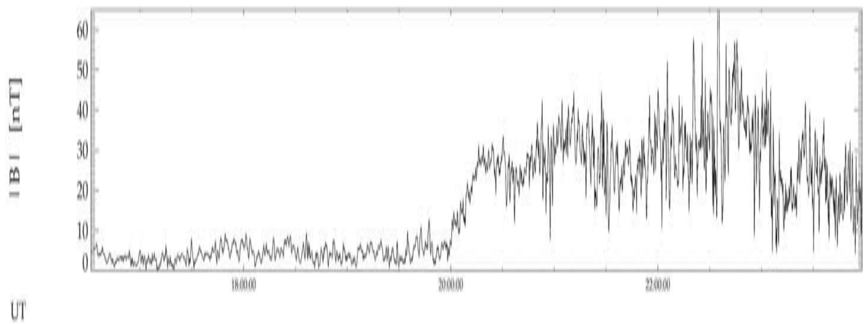

4.1.6 Spektrale Untersuchungen

Von den gemessenen Daten wurden die Leistungsspektraldichte für verschiedene Phasen des Flybys bestimmt. Im Speziellen wurden die Regionen vor und hinter dem Bow Shock unterschieden. Es zeigen sich (s. Folien, Anlage A) ähnliche Frequenzabhängigkeiten für beide Gebiete, jedoch ist das absolute Niveau der Leistungsdichte nach Passieren des Bow Shocks aufgrund vermehrter Turbulenz etwa zwei Grösenordnungen höher. Dieses Ergebnis ist in guter Übereinstimmung mit den Messungen an den Kometen Halley, Giacobini–Zinner und Grigg–Skjellerup.

4.1.7 Gyrofrequenzanalyse

Anhand der erwähnten Spektren wurde die Lage der charakteristischen Maxima als Gyrofrequenzen f_g beteiligter Ionen interpretiert. Gemäß der Beziehung

$$B = 2\pi \frac{m_p}{e} (A f_g), \tag{1}$$

mit dem umgebenden Magnetfeld B, der Protonenmasse m_p, der Elementarladung e und dem Atomgewicht A, sollte bei konstantem Magnetfeld der Graph $B(A, f_g)$ eine waagerechte Gerade sein, wenn die entsprechende Zuordnung der Atomgewichte zu den beobachteten Gyrofrequenzen paßte. Siehe Folien in Anlage A.
Aus diesen Analysen lassen sich z.B. die Wassergruppenionen zweifelsohne identifizieren. Als Nebeneffekt ergibt sich die, wegen der starken magnetischen Störelemente an Bord von DS-1, unbekannte Größe des Magnetfeldbetrages; es bietet sich somit eine neue Art der Inflight Kalibrierungsmöglichkeit bezüglich des Offsets. Ein Vergleich der Magnetfelddatenanalys mit den Ergebnissen des Plasmainstrumentes PEPE ergibt qualitative Übereinstimmung in Bezug auf die detektierten Ionenspecies.

4.2 Plasmasimulation

Mit der am Institut für Geophysik und Meteorologie entwickelten Plasma-Simulation steht ein komplexes numerisches Modell eines Ionentriebwerks zur Verfügung, mit dem die plasmaphysikalischen Phänomene, die mit dem Einsatz von Ionentriebwerken einhergehen, umfassend untersucht werden können. Die bisherigen Anwendungen dieses Codes haben wesentlich zum Verständnis des Neutralisationsregimes beigetragen (siehe Ref. 2 bis 6). Anhand der jüngsten Arbeiten konnte eine verfeinerte Untersuchung der Neutralisation durchgeführt werden (siehe Ref 7,8)

5 Veröffentlichungen und Tagungsbeiträge

Die folgende Liste enthält eine alphabetische Aufstellung der relevanten Deep Space 1 Veröffentlichungen und Tagungsbeitrrage.

1. Brinza D., Henry M., Mactutis A., McCarty K., Rademacher J., van Zandt T., Wang J., Tsurutani B., Katz I., Davis V., Musmann G., Kuhnke F., Richter I., Othmer C., Glaßmeier K.-H., Moses, S.;
   Ion Propulsion Subsystem Environmental Effects on Deep Space One: Initial Results from the IPS Diagnostic Subsystem – DS1 Technology Validation Report; JPL, September 2000

2. Othmer C., Glaßmeier K.-H., Motschmann U., Schüle J., Frick Ch.;
   Three-dimensional simulations of ion thruster beam neutralisation, Phys. Plas., 2000.

3. Othmer C., Glaßmeier K.-H., Motschmann U., Schüle J., Frick Ch.;
   Numerical simulation of ion thruster-induced plasma dynamics, Adv. Space Res., 2000.

4. Othmer C., Motschmann U., Glaßmeier K.-H.;
   Creation of spatial charge separation in plasmas with rigorously charge-conserving local electromagnetic field solvers, J. Comput. Phys., 2000.

5. Othmer C., Glaßmeier K.-H., Motschmann U., Schüle J., Frick Ch.;
   3-D-Simulationen zur Plasmadynamik in der Umgebung eines Ionentriebwerks, Vortrag auf der Tagung der Arbeitsgemeinschaft Extraterrestrischer Forschung (AEF), Bremen, 2000.

6. Othmer C., Glaßmeier K.-H., Motschmann U., Schüle J., Frick Ch.;
   Numerical simulation of the plasmadynamics in the surrounding of an ion thruster, Vortrag auf der Tagung des Committee of Space Research (COSPAR), Warschau, 2000.

7. Othmer C., Glaßmeier K.-H., Motschmann U., Schüle J.;
   Parallel PIC-code simulations of ion thruster -induced plasma dynamics,
   Proceedings of ISSS-6, 2001, Copernicus

8. Othmer C.;
   Numerical simulations of ion thruster-induced plasma dynamics, Dissertation, Institut für Geophysik und Meteorologie, Braunschweig, 2001

9. Rahm M., Kügler. H., Richter I.;
   Fluxgate Magnetometer Calibration for Deep Space 1: Report on the calibration; Institut für Geophysik und Meteorologie, Braunschweig, Februar 1998

10. Rahm M.;
DS–1 Calibration Data Recording System, Interface Document, DS–IGM–TN–0001, Institut für Geophysik und Meteorologie, Braunschweig, Dezember 1997

11. Richter I.;
Fluxgate Magnetometer Analysis for Deep Space 1 : DS–1 Plot System; Institut für Geophysik und Meteorologie, Braunschweig, Februar 1999

12. Richter I.;
Fluxgate Magnetometer Analysis for Deep Space 1 : Long Time Data Investigation; Institut für Geophysik und Meteorologie, Braunschweig, Dezember 1999

13. Richter I., Othmer C., Musmann G., Kuhnke F.,Glaßmeier K.-H., Brinza D.;
Fluxgate Magnetometer Data Analysis of the Deep Space 1 Satellite Mission;
Vortrag auf der Tagung der European Geophysical Society (EGS) in Den Haag, April 1999

14. Richter I., Glaßmeier K.-H., Musmann G., Kuhnke F., Othmer C.;
Analyse von Magnetometerdaten auf der Deep Space 1 Satellitenmission; Vortrag auf der Tagung der Arbeitsgemeinschaft für Extraterrestrische Forschung (AEF) in Bremen, März 2000

15. Richter I., Othmer C., Kuhnke F., Musmann G., Glaßmeier K.-H., Vogt J., Brinza D., Tsurutani B.;
Magnetometer Observations During the Flyby of Deep Space 1 at the Asteroid Braille; Vortrag auf der Tagung der American Geophysical Society (AGU) in Washington, Mai 2000

16. Richter I., Othmer C., Musmann G., Kuhnke F.,Glaßmeier K.-H., Brinza D.;
Magnetic Field Measurements During the Encounter of DEEP SPACE 1 at the Comet Borrelly
Vortrag auf der Tagung der European Geophysical Society (EGS) in Nizza, April 2001

17. Richter I., Brinza D., Cassel C., Glaßmeier K.–H., Kuhnke F., Musmann G., Othmer C., Schwingenschuh K., Tsurutani B.;
First Direct Magnetic Field Measurements of an Asteroidal Magnetic Field: DS1 at Braille GRL, Vol 28, No 10, May 15, 2001

18. Richter I., Brinza D., Glaßmeier K.–H.,Henry. M, Kuhnke F., Musmann G., Othmer C., Schwingenschuh K., Tsurutani B.;
Magnetic Field Measurements During the Encounter of DEEP SPACE 1 at the Comet Borrelly, GRL, to be published

Die Arbeit von Dr. Günter Musmann, Dr. Falko Kuhnke, Dr. Carsten Othmer, Dr. Ingo Richter, und Prof. Dr. K.–H. Glaßmeier wurde vom Bundesministerium für Bildung und Wissenschaft und vom Deutschen Zentrum für Luft– und Raumfahrt gemäß Förderungsvertrag 50 OO 0102 finanziell unterstützt.

Magnetic Field Measurements During the Encounter of DS1 at the Comet Borrelly

EGS Meeting, Nice, April 20, 2002

Ingo Richter

K.–H. Glassmeier
F. Kuhnke
G. Musmann
C. Othmer
J. Vogt
D. Brinza (JPL)
B. Tsurutani (JPL)

Institute for Geophysics and Meteorology
TU–Braunschweig, Germany

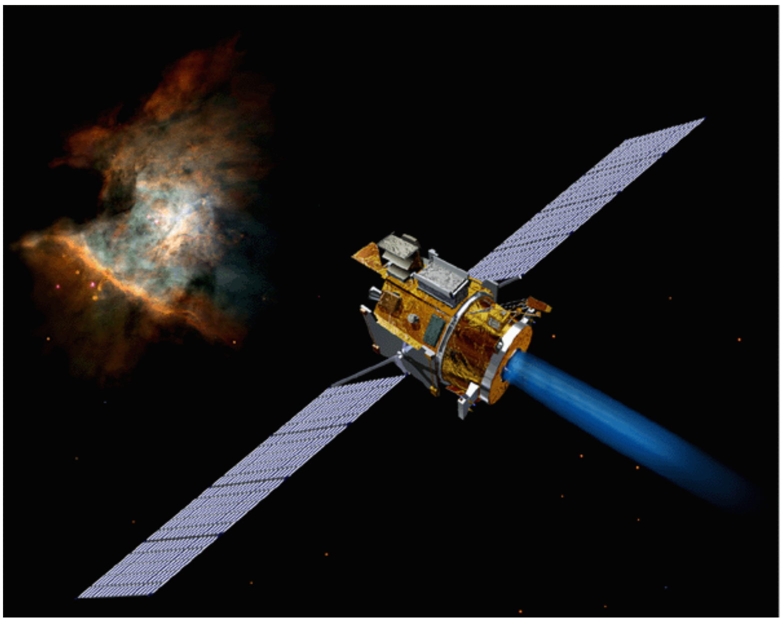

Milestones of the DEEP SPACE 1 Mission

- **Launch: October 24th, 1998, Cape Canaveral**
- **1. Goal: Flyby at the asteroid Braille, July 29th 1999**
  ⇝ Magnetometer revealed Asteroidal Magnetic Field
- **2. Goal: Encounter at comet Borrelly**

Date:	September 22nd, 2001
Distance:	2170km, 1.36 AU
Relative Velocity:	16.5 km/s

  ⇝ Magnetometer revealed typical Cometary Magnetic Field structure

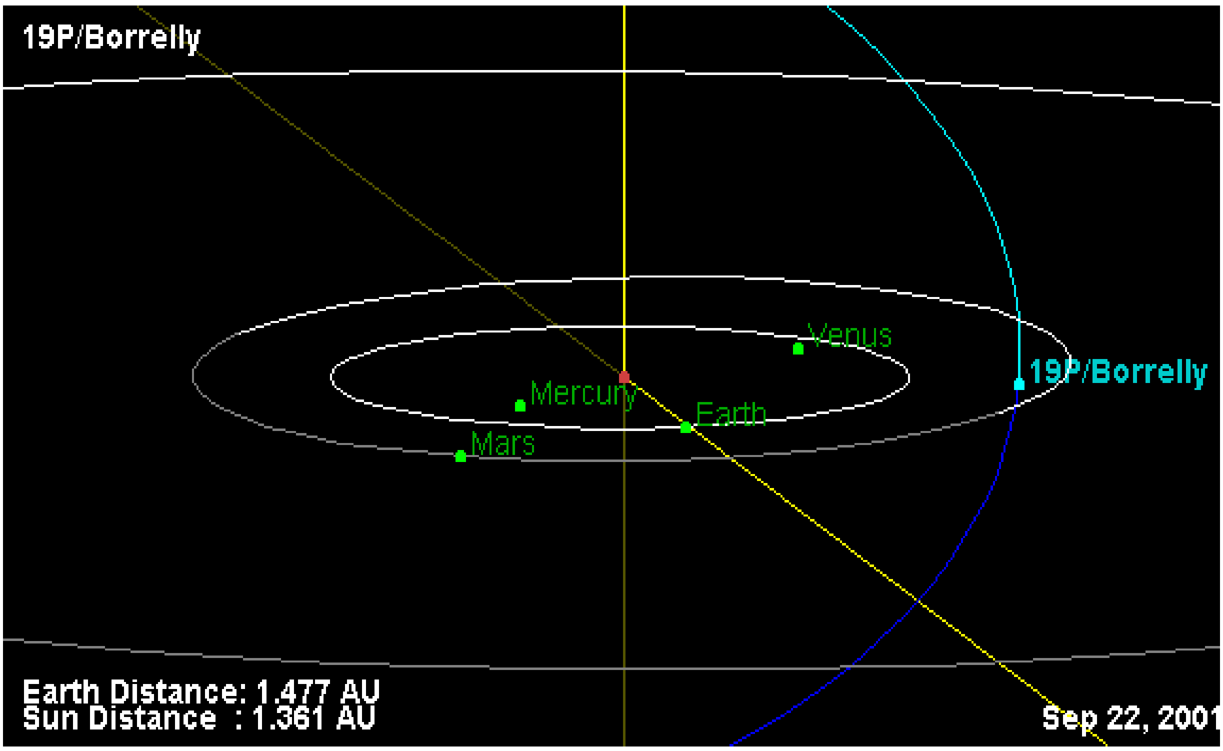

The Fluxgate–Magnetometer of the TU–Braunschweig

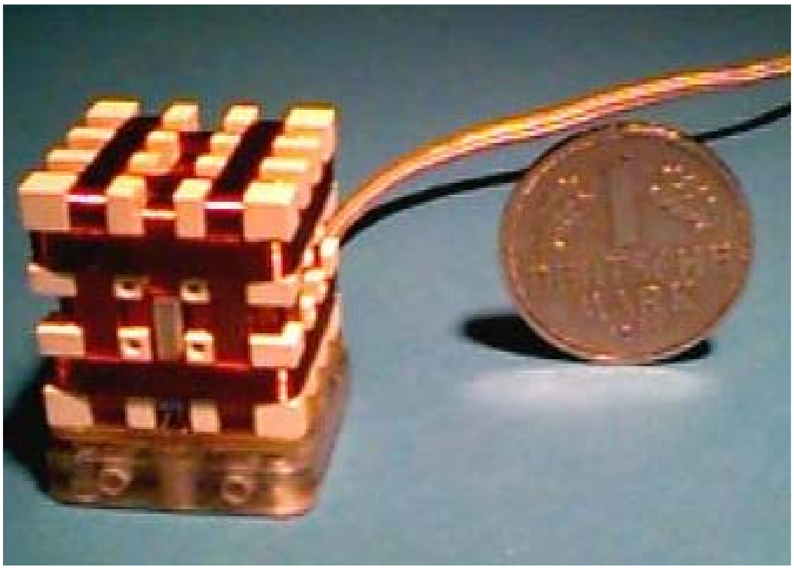

- **2 Sensors**
- **Operating Range: ±25000 nT**
- **Resolution: 0.04 nT (20 Bit ADC)**
- **Sample frequency: 20 Hz (burst mode)**
  1 Hz (scan mode)

2×

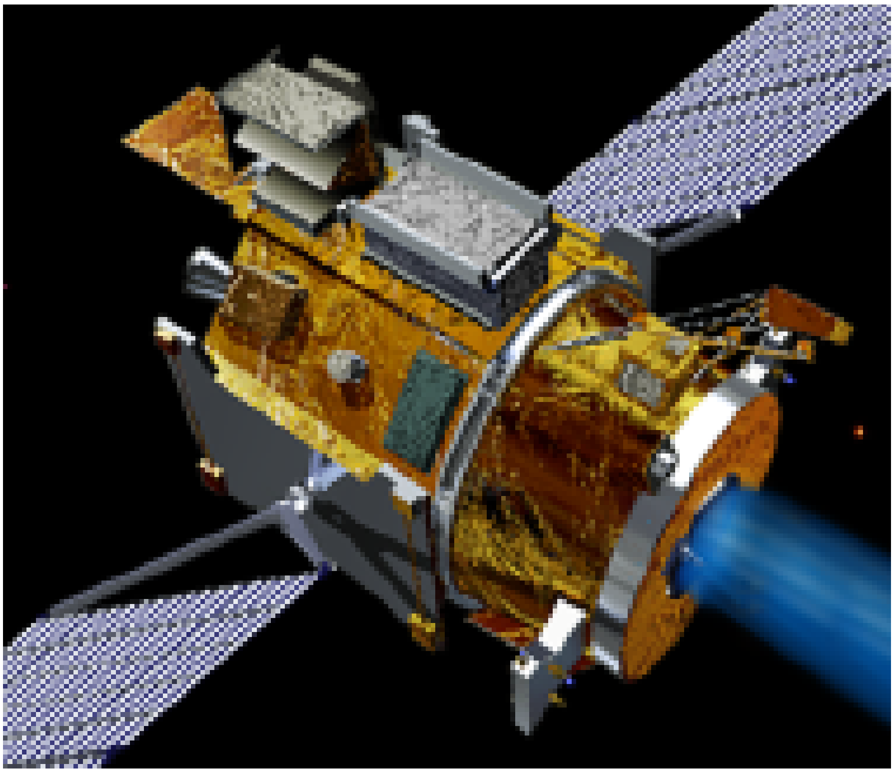

DS1 FGM Data Analysis Procedure

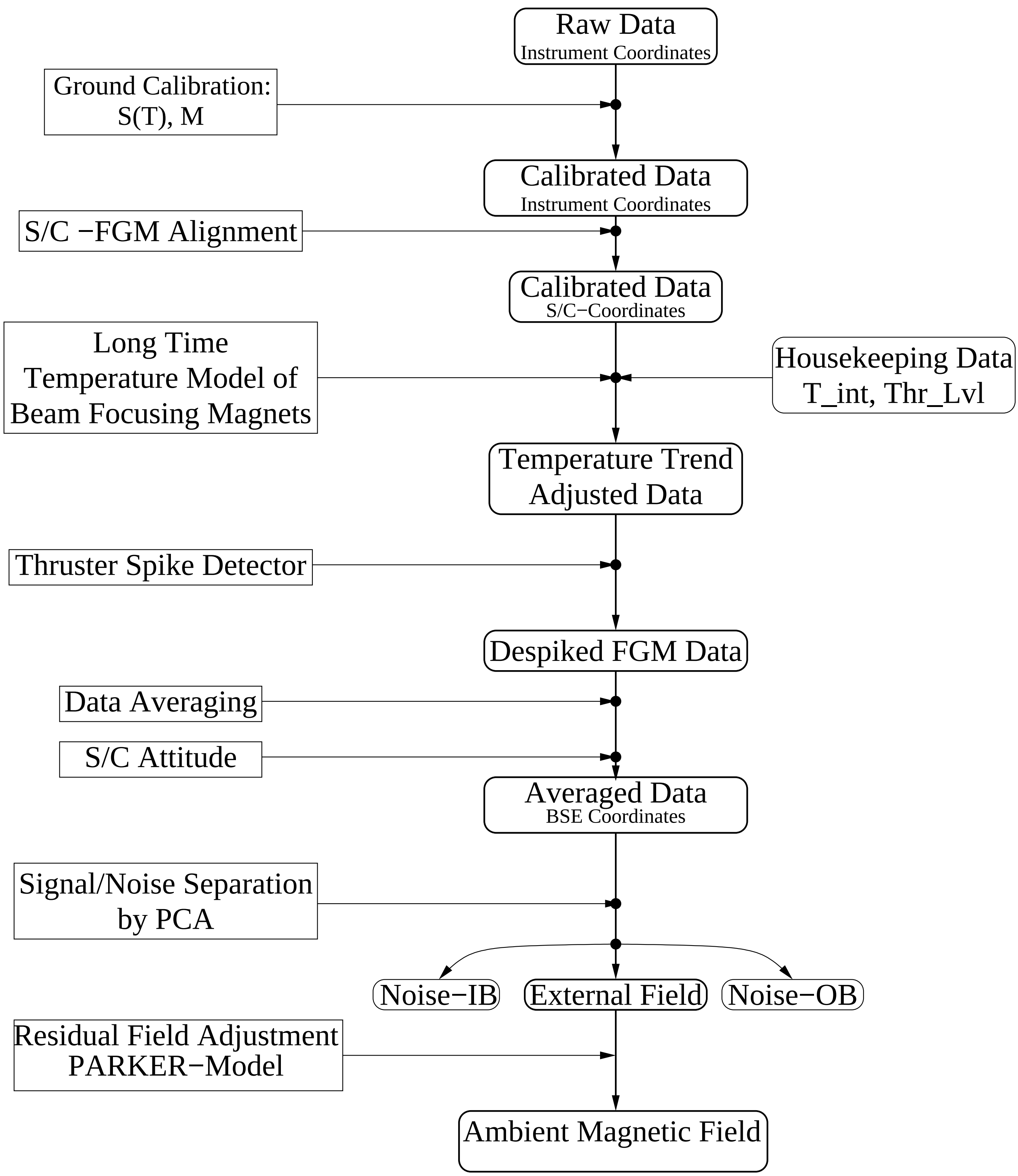

DS1–Borrelly Fly By Trajectory

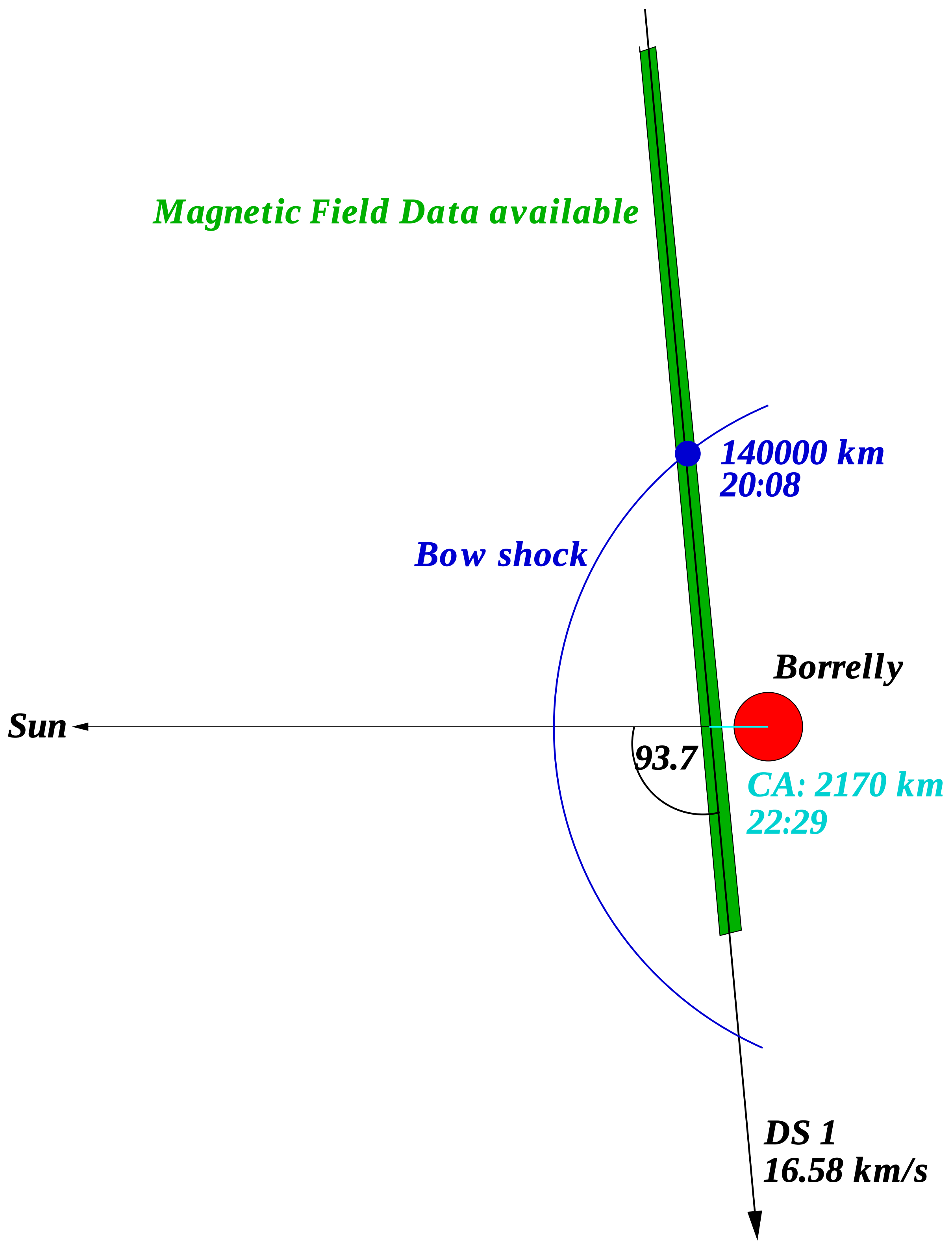

Calibrated, Averaged Scan Data in BSE Coordinates

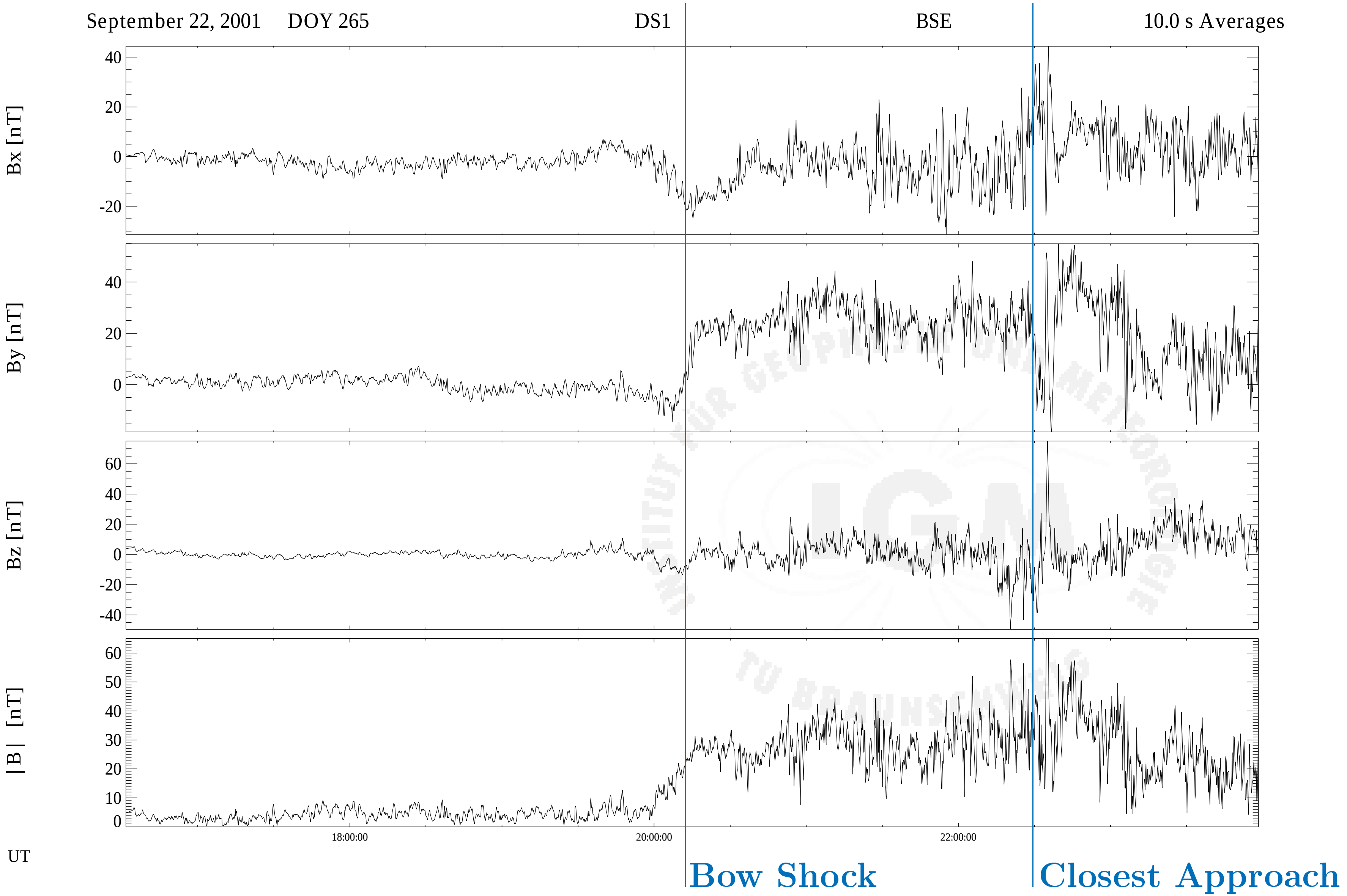

Remark: Residual Fields adjusted to estimated PARKER fields

The Fly By Geometry and Magnetic Field Direction

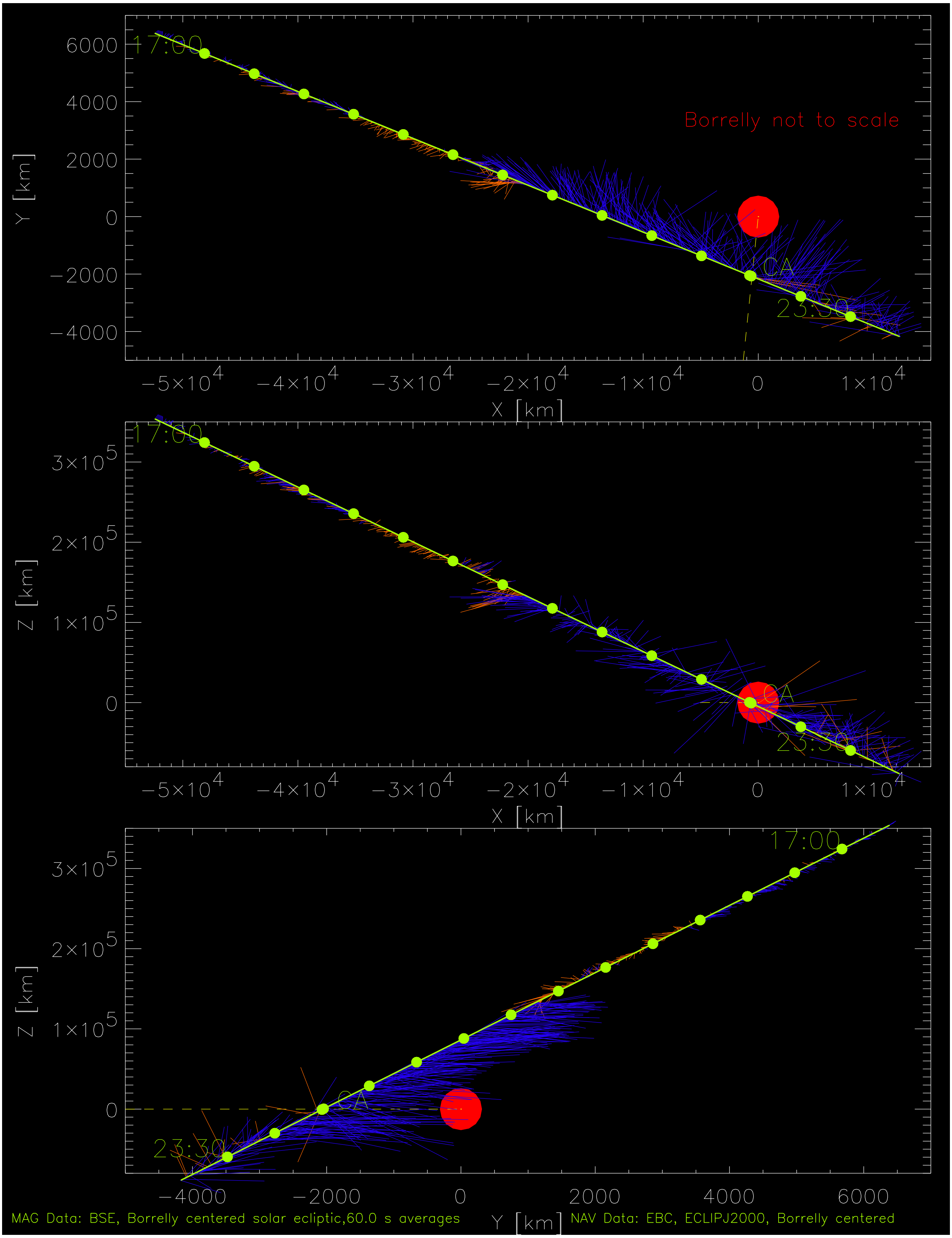

Burst Data in Vicinity of the Closest Approach

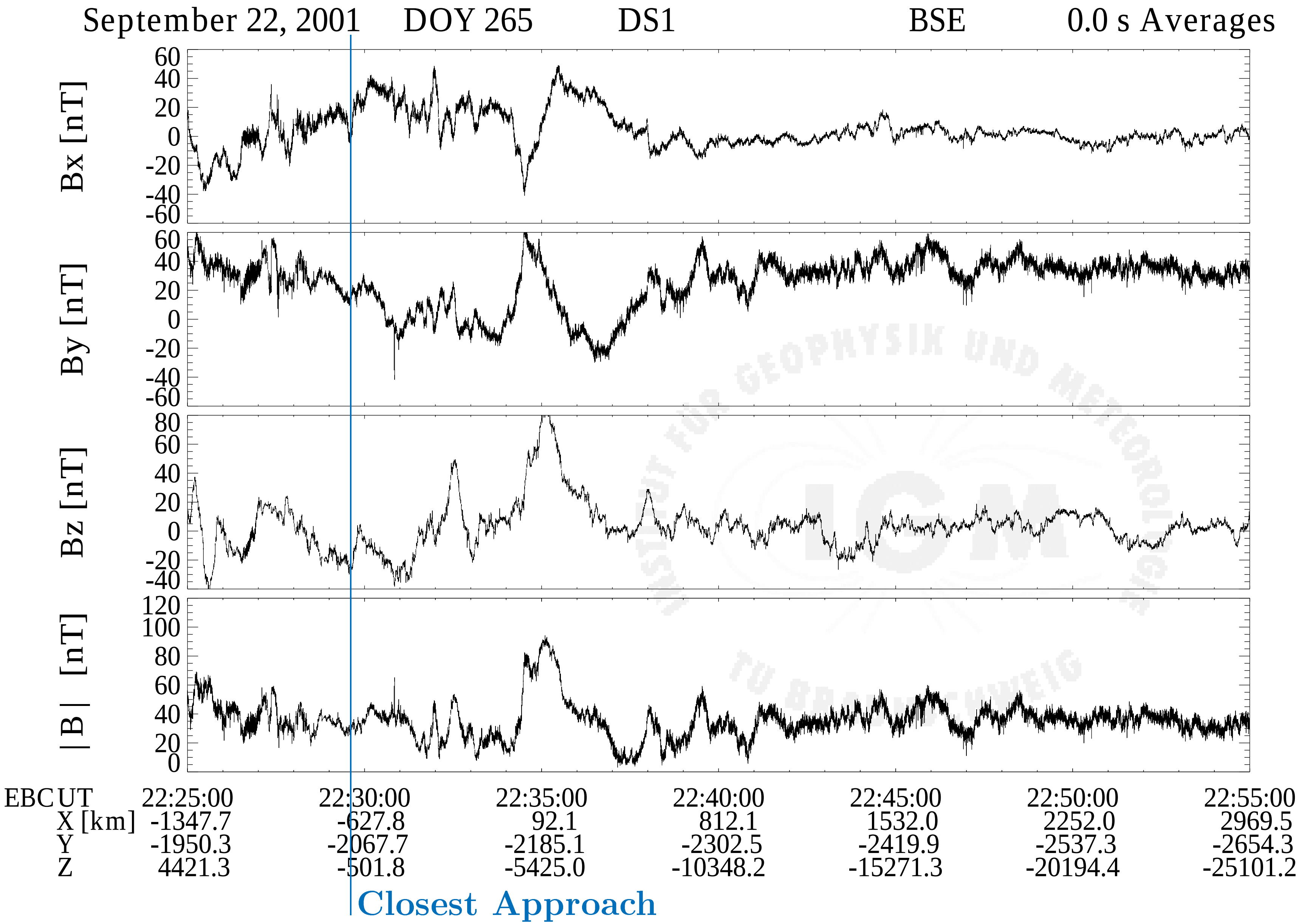

Remark: Residual Fields adjusted to estimated PARKER fields

Power Spectra in Front & Beyond Bow Shock

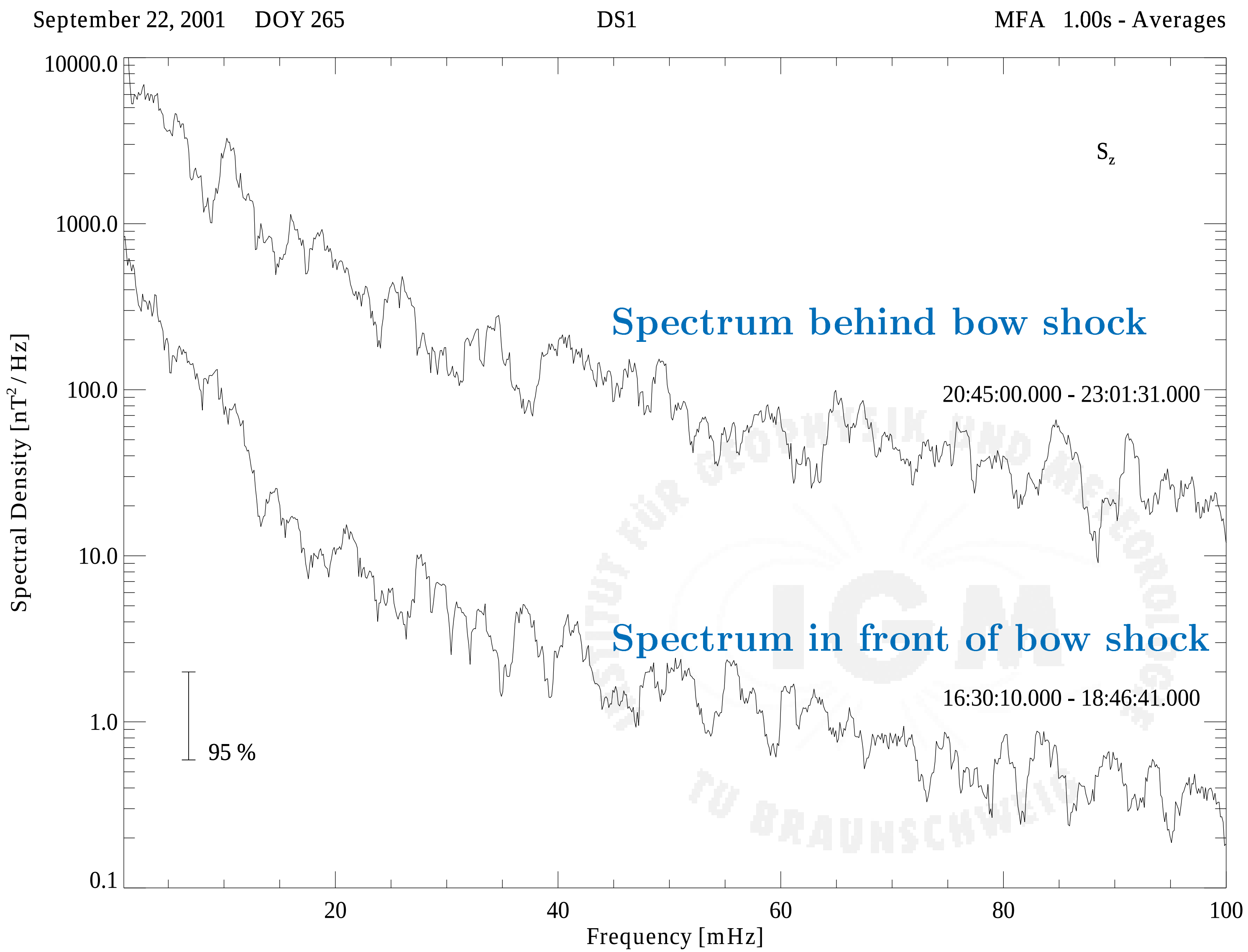

Power Spectra in Front & Behind Bow Shock

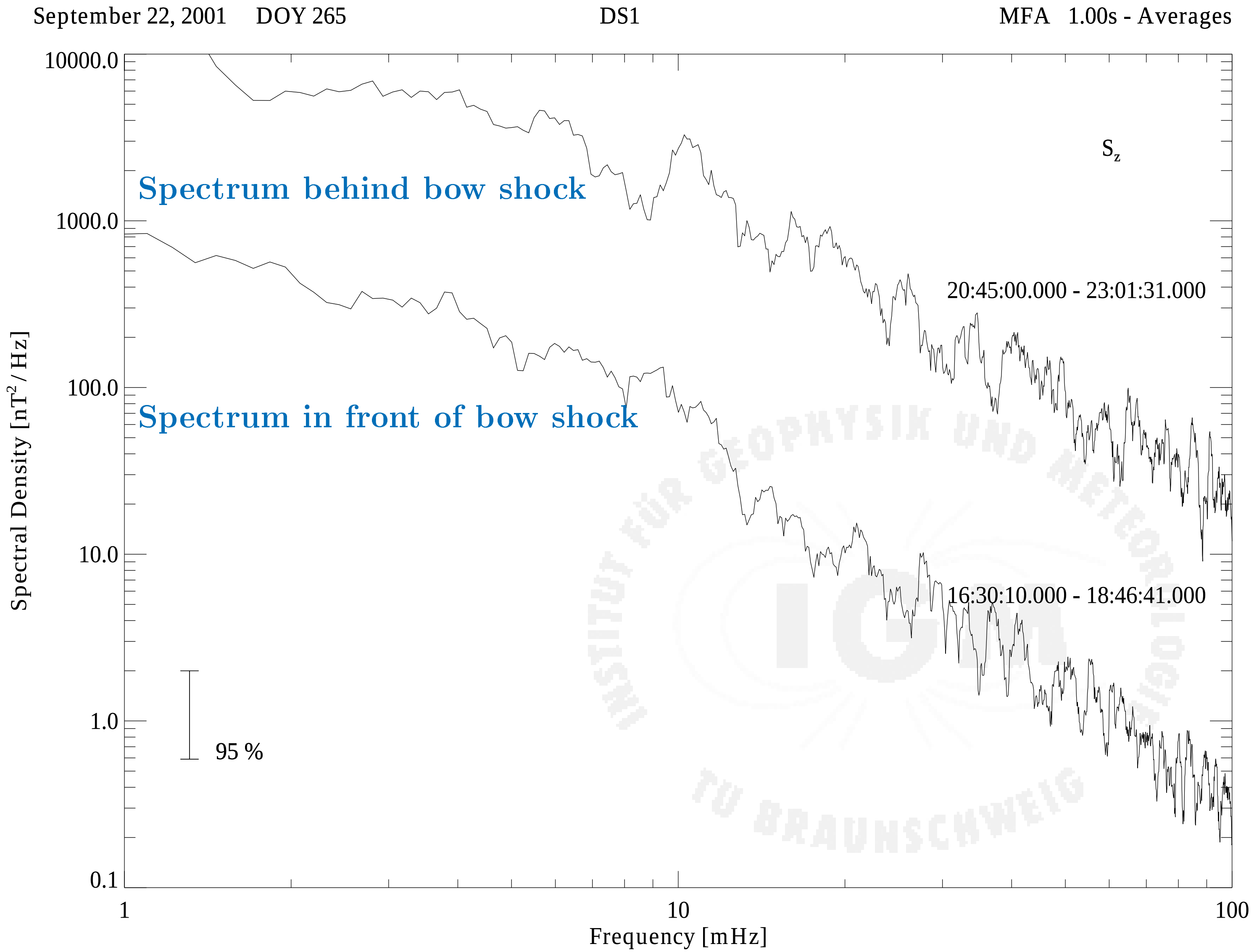

Gyrofrequency Analysis

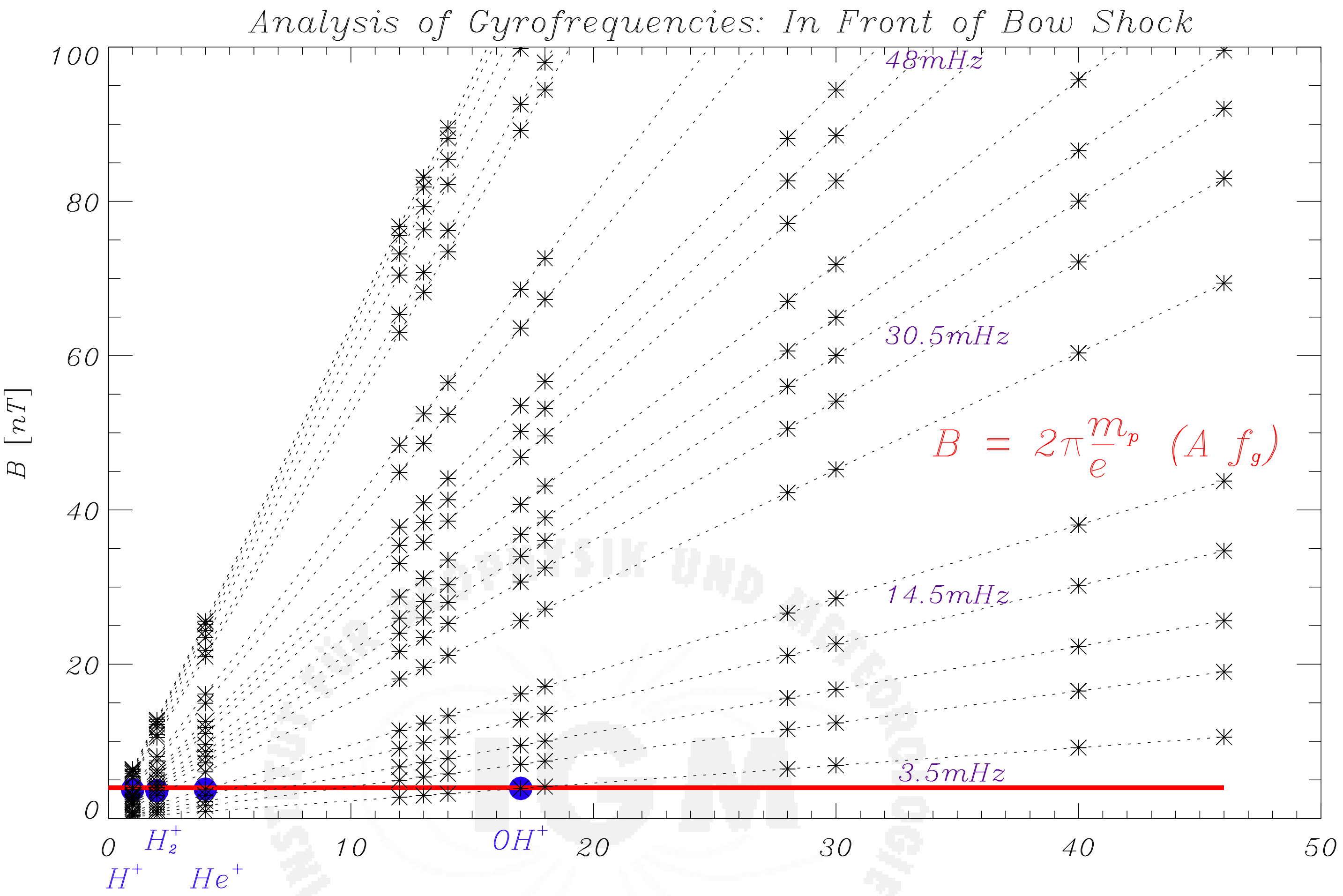

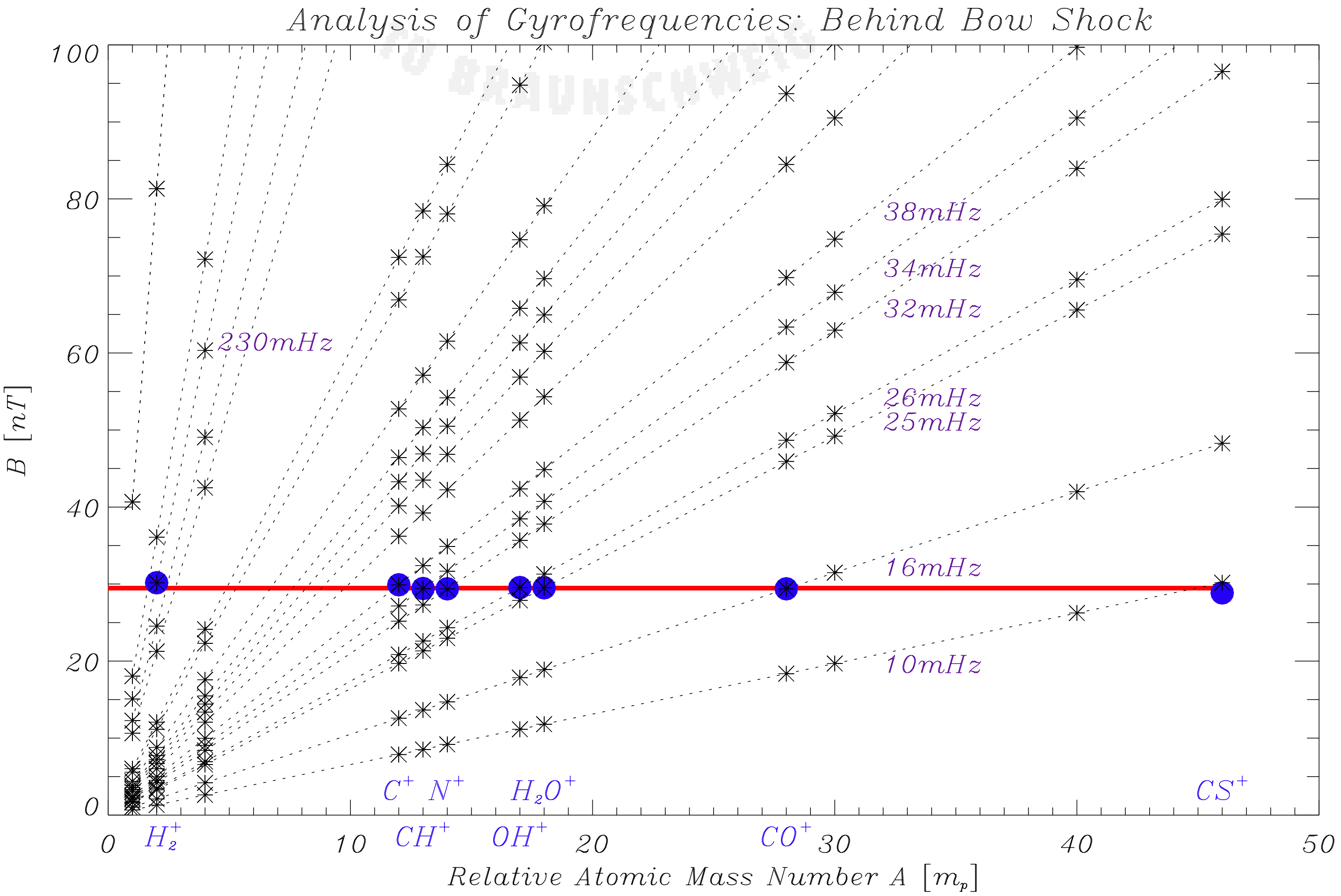

Dynamic Spectrum of the Magnetic Field

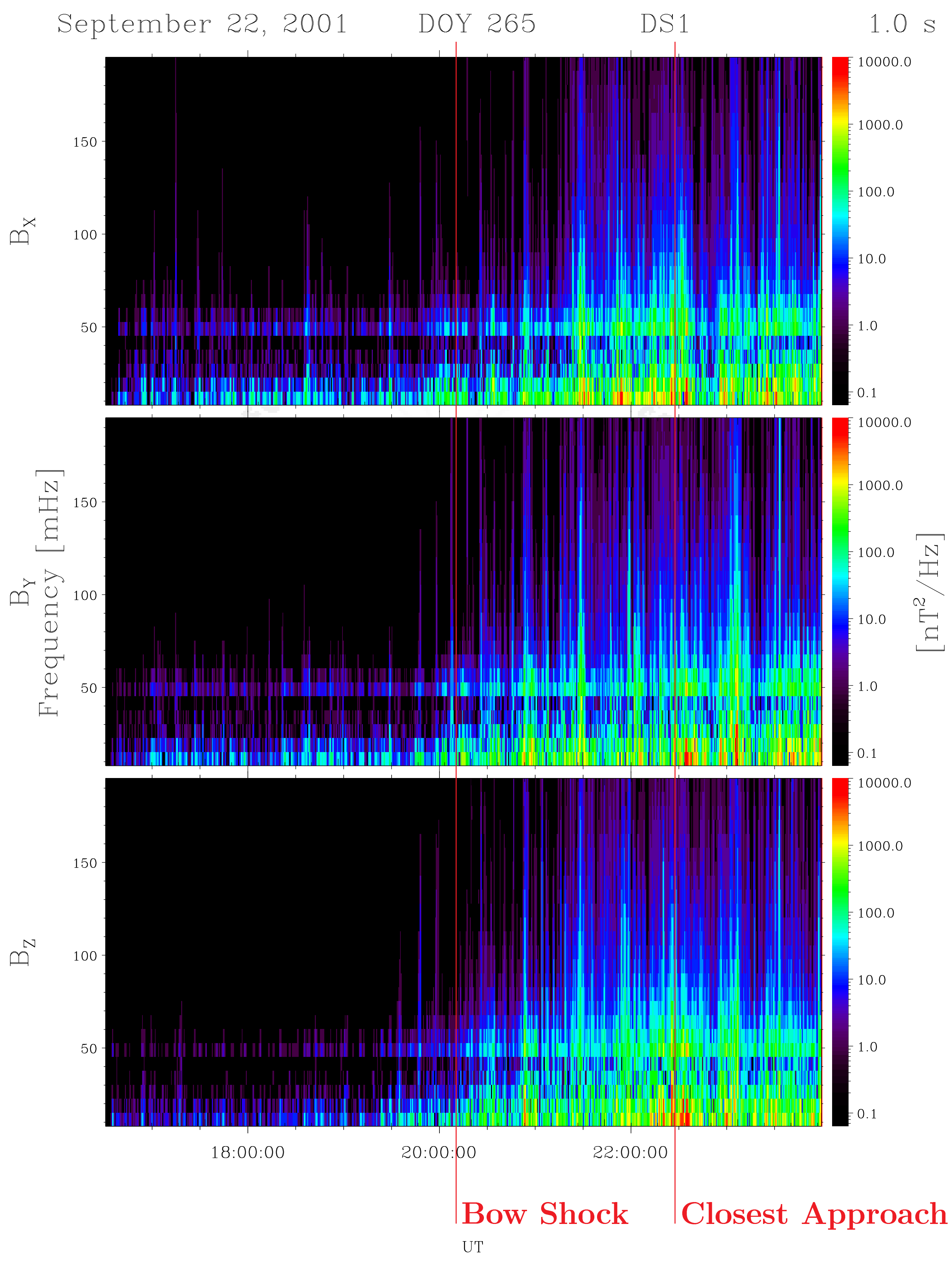

Magnetic Field Measurements during Comet Fly Bys

Giotto @ Halley
March 13, 1986

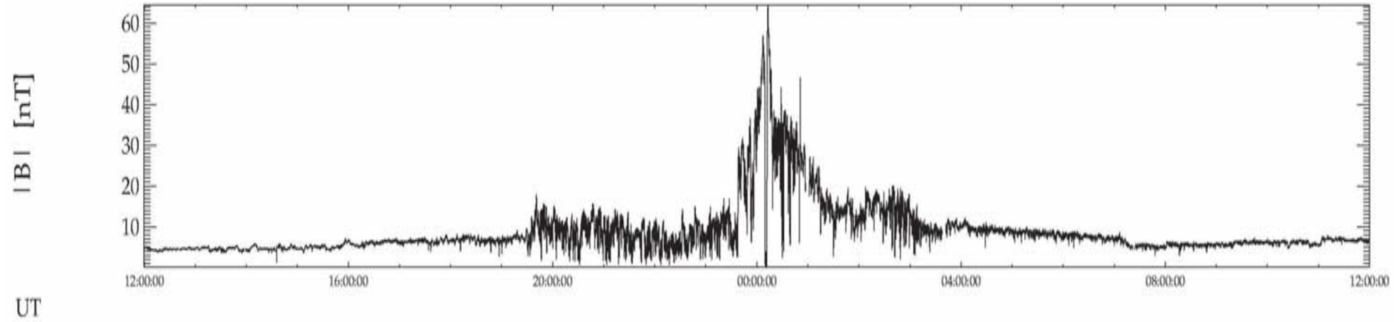

Giotto @ Grigg-Skjellerup
July 10, 1992

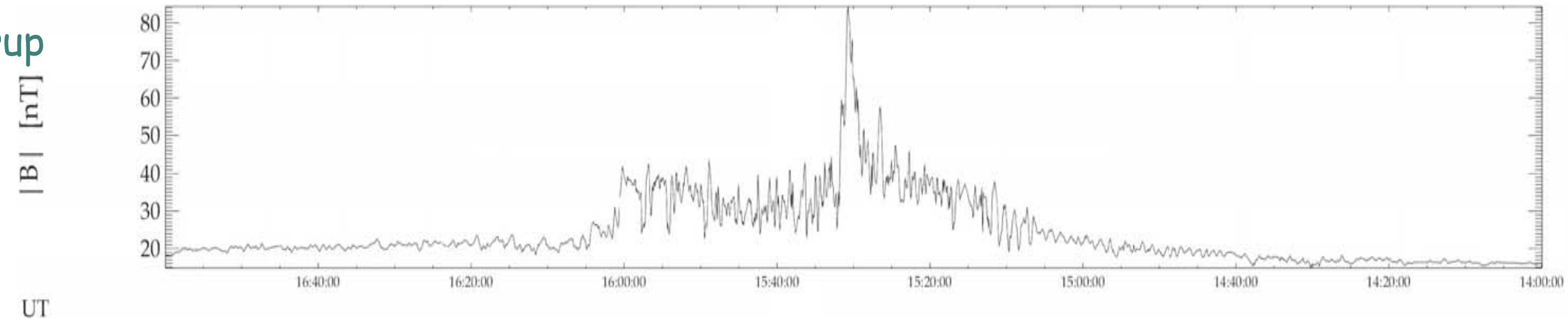

ICE @ Giacobini-Zinner
September 11, 1985

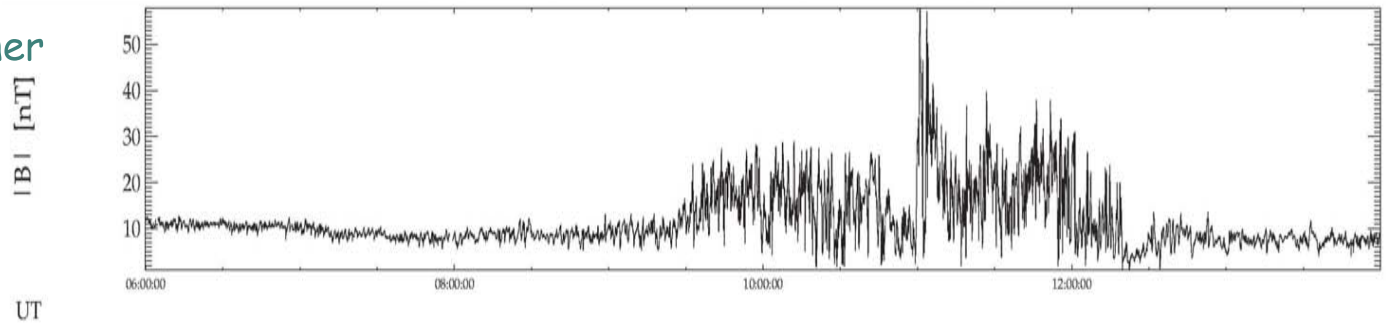

Deep Space 1 @ Borrelly
September 22, 2001

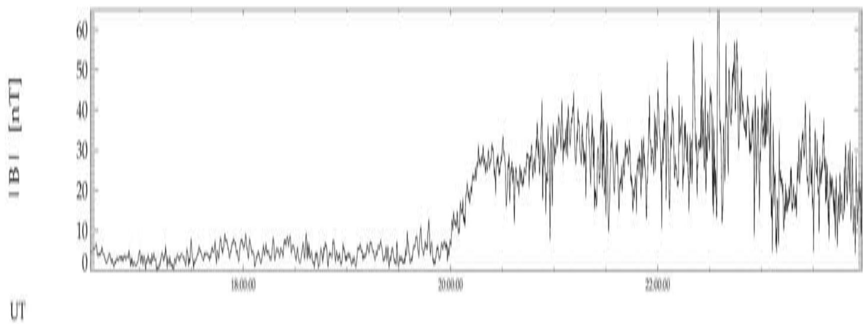

Borrelly & Other Comets

		Giacobini-Zinner	Halley	Grigg-Skjellerup	Borrelly
				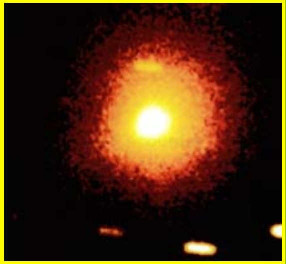	
		ICE	Giotto	Giotto	Deep Space 1
		11.09.1985	13.03.1986	10.07.1992	22.01.2001
Fly By Trajectory		Tail	Upstream	Tail	Upstream
CA distance	Rca [km]	7862	596	200	2172
CA velocity	vca [km/s]	20.7	68.7	14.0	16.6
Gas production rate	Q [1/s]	3.00E+28	1.00E+30	3.60E+27	2.90E+28
Contact surface Distance	Rcs [km]	317	5245	68	412
Perp. Bow Shock Distance	Rperp = 1.5 RSub [km]	111000	1153500	9900	140700
Max. Magnetic Field	Bmax [nT]	60	65	85	65

GEOPHYSICAL RESEARCH LETTERS, VOL 28, NO. 10, PAGES 1913-1916, MAY 15,2001

First Direct Magnetic Field Measurements of an Asteroidal Magnetic Field: DS1 at Braille

I. Richter,[1] D. E. Brinza,[2] M. Cassel,[3] K.–H. Glassmeier,[1] F. Kuhnke,[1] G. Musmann,[1] C. Othmer,[1] K. Schwingenschuh[4] and B. T. Tsurutani[2]

Abstract. Deep Space 1 (DS1) is the first interplanetary spacecraft (s/c) using ion propulsion and aims at investigating the compatibility of innovative technology with scientific measurements. DS1 performed a successful flyby at the asteroid Braille on July 29th, 1999. This closest-ever encounter allowed for the first time a direct measurement of an asteroidal magnetic field. The manifold magnetic disturbances caused by the ion propulsion onboard DS1, however, required an elaborate data processing scheme in order to extract the magnetic signature of Braille. Its successful application to the magnetometer data of the asteroid flyby reveals a magnetic moment of $2.1 \cdot 10^{11} \mathrm{Am}^2$ for Braille.

Mission Overview

Asteroidal research reveals essential secrets about the structure and the history of our universe. The genesis of the universe can be studied by investigating the asteroidal composition, which may be obtained from magnetic field measurements. The most likely source of asteroidal magnetic fields is remnant magnetization initially caused by a dynamo in the asteroid's parent body and frozen in during its cooling. Thus, asteroids with strong magnetic fields are believed to be fragments of larger parent bodies.

A unique opportunity of dealing with such issues is given by an asteroid flyby like the encounter of DS1 at 9969 Braille. The DS1 mission [*DS1 Press Kit*, 1999] is the first mission of NASA's New Millennium Program. This program was created to test and to validate outstanding technologies for the future space exploration of the 3rd millennium. DS1 was launched successfully on October 24th, 1998 at the Kennedy Space Flight Center, Cape Canaveral. The most remarkable feature of DS1 is the first use of an ion propulsion system during a deep space mission.

DS1 is equipped with ion engine diagnostic sensors [*Brinza et al.*, 2000] including two ultra small 3-axes high-resolution fluxgate magnetometers (FGM). This instrument, which is the prototype of the ROSETTA magnetometer [*Glassmeier*, 2001], has been developed at the Institute for Geophysics and Meteorology in Braunschweig. It has been designed for the extremely high requirements in space: the instrument with a wide measurement range of ±25000 nT (due to the intrinsic s/c field) is able to resolve the magnetic field with a resolution of 0.04 nT. It can operate in a temperature range of −150°C to +300°C. In spite of the high vector rate of 20 Hz it just consumes 200 mW power.

The primary scientific mission objective was a rendezvous with the asteroid 9969 Braille [*Hicks et al.*, 1999] (formerly temporarily called 1992 KD) on July 29th, 1999. The closest approach (CA) [*Soderblom et al.*, 1999] took place at a distance of 1.3 AU from the sun. This asteroid encounter was the closest flyby (28 km) to a celestial body ever achieved by a spacecraft. DS1's orbit is inclined 0.3° from the ecliptic, whereas Braille's inclination is 28°. The CA occurred on Braille's ascending node. DS1 passed Braille on the nightside with a relative velocity of 15 km/s. Therefore the duration of stay at Braille's wake region was only 0.13 s. The magnetic field data taken during this flyby led to the first magnetic characterization of the asteroid Braille.

Description of the Data Processing for the Encounter Data

The two FGMs of DS1 are located outside the s/c on a 50 cm long boom (close to the ion engine beam for additional diagnostic purposes). At this short distance the FGMs are strongly influenced by the temperature dependent ion engine permanent magnets, the ion beam itself, and the thrusters

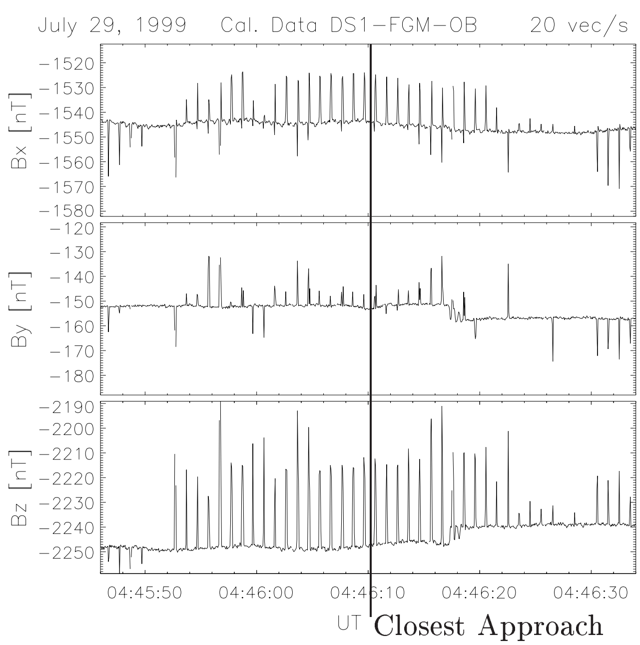

Figure 1. Calibrated raw data of the outboard magnetometer FGM-OB in s/c coordinates.

[1]Institute for Geophysics and Meteorology, TU Braunschweig, Germany

[2]Jet Propulsion Laboratory, California Institute of Technology, Pasadena, CA.

[3]Institute for Computer and Communication Network Engineering, TU Braunschweig, Germany.

[4]Institute for Space Research, TU Graz, Austria.

Paper number 2000GL000000.
0094-8276/01/2000GL000000$05.00

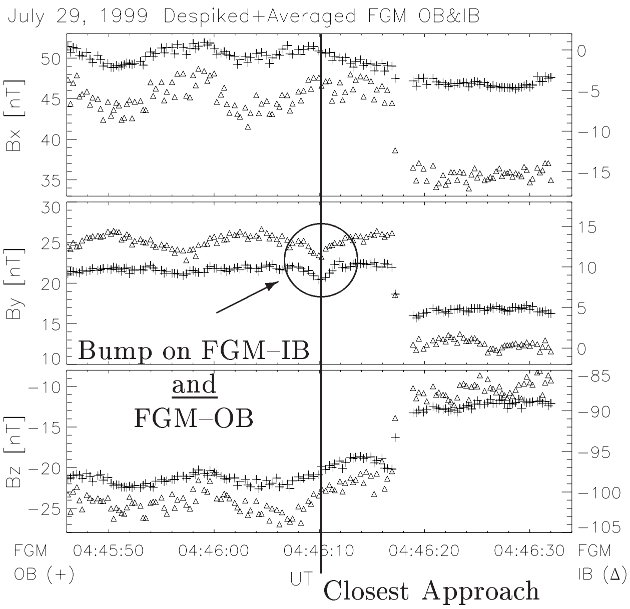

Figure 2. 0.2 s averages of the temperature corrected and despiked OB(+) & IB(Δ) data in s/c coordinates.

(magnetically activated) used for attitude control of the s/c. Due to these circumstances an extensive data analysis procedure has to be applied to achieve significant scientific data out of the raw data.

The instruments measure raw data in sensor coordinates. In the first step of the analysis the results of the instrument ground calibration, namely the temperature dependent sensitivity, the misalignment and the offsets of the sensors, have to be taken into account to generate calibrated data. Afterwards the data have to be transformed from sensor coordinates to s/c coordinates using the mounting matrices. For the time of the CA the orientation of the orthogonal s/c system with respect to the sun is defined by the sun-body-vector $(24.93°, 89.97°, 65.07°)$, whose components are the angles between the s/c coordinate axes x, y, z and the direction to the sun. Figure 1 shows these preprocessed data for a 50 s interval around the CA at Braille.

Three major features can be perceived from the data: the huge residual fields caused by the ion engine permanent magnets, the spikes originating from the attitude controlling thrusters and a discontinuity of about 7 nT 7 s after CA. This huge jump is artificial and caused by switching off a 100 W heater onboard DS1 at 04:46:17 UT. The residual fields can be eliminated by applying the temperature model of the ion engine permanent magnets. Such a model has been developed using calm phases of the magnetic field in a period of half a year for different temperatures of the ion engine. This long term monitoring revealed component specific linear dependencies of the residual field on the internal engine temperature T_{int}. The temperature dependencies are of the order of -1.2 nT/K…2.3 nT/K. Especially the x and z components show huge temperature variations. This is most likely caused by the complex geometry and orientation of the ion engine permanent magnets in relation to the magnetometer positions on the tilted boom. After application of this model the magnetic field data are temperature trend corrected.

Generally, at this step of the analysis the influence of the ion beam had to be eliminated. However, the ion engine was deactivated 48 hours before the closest approach and subsequent maneuvers were performed by conventional hydrazine thrusters. Thus an ion beam correction does not have to be considered here.

Now the spikes have to be eliminated by a despiking algorithm, using a shortterm/long-term average filter. About 0.3 s of a 1 s time interval are corrupted by the “thruster signature”. These sections are detected and set to the local average of the undisturbed phases. After the subsequent averaging (0.2 s mean) the data shown in Figure 2 are obtained. The most remarkable feature of this plot is a bump appearing on the data of the outboard (OB) as well as on the inboard (IB) FGM with the same amplitude (therefore, of external origin in contrast to the internal heater caused discontinuity at 04:46:17 UT occurring in different amplitudes on both FGMs) exactly at the time of the CA at the asteroid. This seems to be an indication of a magnetic signature of Braille. For a proof of this hypothesis the separation of s/c generated noise and the external field has to be executed. This can be achieved by a Principal Component Analysis (PCA) [*Chatfield and Collins*, 1980; *Holmes et al.*, 1996]. This algorithm splits the external field, which occurs correlated with the same amplitude in both sensors, from the s/c generated noise, which shows up, due to the r^{-3} decay of magnetic dipole fields, in different amplitudes on both sensors. The method utilizes the feature that the s/c noise and the external field are uncorrelated. After the application of this procedure the variations in the obtained external field data are diminished to the order of a few nanotesla; the suspicious bump, however, remains on the B_y component of the decomposed signals.

For the next step of the analysis just the data in a 6 s interval around the CA will be investigated. This set of data

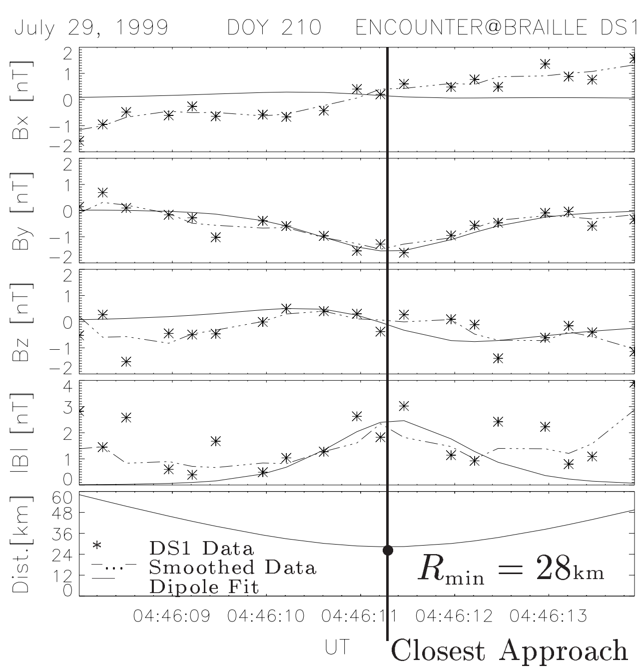

Figure 3. Zoomed extracted external field data for the encounter in a distance of $R_{\text{min}} = 28$ km at Braille. The dipole fit reveals a moment of $2.1 \cdot 10^{11}$ Am^2.

Table 1. Characteristics of Selected Asteroids. (Values in brackets have been derived from material properties as there were no flyby data available.)

ASTEROIDS	**VESTA**	**MATHILDE**	**IDA**	**EROS**	**GASPRA**	**BRAILLE**
Dimension [km]	$\emptyset : 530$	$66 \times 48 \times 46$	$60 \times 25 \times 19$	$33 \times 13 \times 13$	$18.2 \times 10.4 \times 9.4$	$2.2 \times 1 \times 1$
Equivalent Radius [km]	265	26	16	9	8.0	0.78
Volume [km^3]	$7.8 \cdot 10^7$	77000	16100	2600	2145	2
Density [kg/m^3]	3900	1340	2600	2700	3900	3900
Material	Basalt Pyroxene Olivine	Carbonaceous Chondrites	Olivine Orthopyroxene	LL–Chondrites randomly magnetized Chondrules	Metal Olivine Pyroxene	Basalt Pyroxene Olivine
Spectral Class	S/U-Class	C-Class	S-Class	S-Class	S-Class	Q/S-Class
Mass [kg]	$3.04 \cdot 10^{20}$	$1.03 \cdot 10^{17}$	$4.19 \cdot 10^{16}$	$7.02 \cdot 10^{15}$	$8.36 \cdot 10^{15}$	$7.80 \cdot 10^{12}$
Shape	Sphere	Lump	Croissant	Banana	Potato	Peanut
Periheldistance [AU]	2.15	1.94	2.73	1.13	1.82	1.33
Apheldistance [AU]	2.57	3.35	2.99	1.78	2.59	3.36
Orbital Period [year]	3.63	4.31	4.84	1.76	3.29	3.58
Rotational Period [d]	0.22	17.40	0.19	0.22	0.29	9.4
Encounter		NEAR: 27.7.97	Galileo: 28.8.93	NEAR:14.2.00	Galileo: 29.10.91	DS1: 29.07.99
Encounter Distance R [km]		1212	2700	15 (Orbit)	1600	28
Magnetic Field [nT] @ R		(0.86)	(0.016)	≈ 0	(0.01)	2
Max. Dipole Moment [Am^2]	$(7.8 \cdot 10^{18})$	$(7.7 \cdot 10^{15})$	$(1.6 \cdot 10^{15})$	?	$2.0 \cdot 10^{14}$	$2.1 \cdot 10^{11}$
Max. Magnetization [A/m]	(100)	(100)	(100)	?	93	110
Max. Surface Field [nT]	(83776)	(83697)	(83776)	≈ 0	78125	92517
Spec. Moment [A m^2/kg]	(0.026)	(0.075)	(0.038)	?	0.024	0.028

is displayed in Figure 3. The asterisks mark the data, the dashed-dotted lines represent smoothed data and the solid lines are the result of a dipole fit. The plotted field modulus is just the root of the sum of the shown squared components. With the fit-software a dipole with a fixed position at the center of the asteroid, but variable orientation and magnetic moments was detected. An additional observed linear trend on the x-component (3 nT/6 s), probably caused by a slowly changing solar wind, was included in the model. The obtained best fit revealed a dipole moment of Braille of $2.1 \cdot 10^{11}\,Am^2$. The quality, represented by the cross correlation between the fit and the smoothed data is 0.96, 0.92, 0.41 for the the B_X, B_Y and B_Z component. The fitted dipole has an orientation of 235° azimuth (XY-Plane) and 105° elevation (angle with z axis) in the s/c system defined above. Unfortunately there are no data available, which relate the figure axis of Braille to the s/c coordinate system.

Comparison with other Asteroids

To assess this result in a wider scope the known characteristic data of the asteroids 433 Eros, 951 Gaspra, 243 Ida, 253 Mathilde and 4 Vesta were considered. Table 1 gives an overview about the characteristics of these asteroids (taken from the www sites listed in Table 2). Gaspra and Braille are the only ones which have been investigated in terms of the magnetic field yet. The characteristic magnetic quantities of Gaspra have been estimated using magnetometer data and the assumption of the asteroid's interaction with the solar wind [*Kivelson et al.*, 1994; *Baumgaertel et al.*, 1994, 1997]. Those considerations showed that the solar wind is draped around a region being much larger than Gaspra. Therefore, Gaspra seems to build up a magnetospheric obstacle in the solar wind which affects the magnetic field measurements. The situation at Braille, however, is a completely different one. As the volume of Braille is just a thousandth of that of Gaspra, it does not act as a significant obstacle for the solar wind. Additionally Gaspra is thought to be more metallic than Braille. To achieve a quantitative statement, Greenstadt's conditions for asteroidal magnetospheres [*Greenstadt*, 1971] can be applied to Braille. As a result, just two of the three necessary conditions for generation of a magnetosphere are met. The magnetic field of Braille which should stop the solar wind in a certain stopping distance is large enough and also the stopping distance is of the right order. The third condition, however, the minimum surface field for lateral stability of a putative magnetosphere, had to be two orders of magnitude higher. Thus, Braille cannot build up a magnetosphere, and the measured field is just the unperturbed dipole field of the asteroid. Due to these

Table 2. Selected Asteroid Data WWW–Sites

Asteroid	URL
General	•planetscapes.com/solar/germ/asteroid.htm •www.astro.uio.no/ita/DNP/nineplanets /asteroids.html •nssdc.gsfc.nasa.gov/planetary/factsheet /asteroidfact.html •spacelink.msfc.nasa.gov/Instructional.Materials /Curriculum.Support/Space.Science /Our.Solar.System/Solar.System.Lithograph.Set /Asteroids/index.html •spdext.estec.esa.nl/content/doc/02/2306_.htm
EROS	•www.amsky.com/0300/near/near.html •www.spacescience.com/headlines/y2000 /ast19feb_1.htm •www.jhuapl.edu/public/pr/000217.htm •nssdc.gsfc.nasa.gov/planetary/text/eros.txt
GASPRA	•www.astro.washington.edu/smith/Astro150 /Worlds/Asteroids.html
IDA	•www.jpl.nasa.gov/galileo/slides/slide18.html •www.wappswelt.de/tnp/nineplanets/ida.html
MATHILDE	•near.jhuapl.edu/Mathilde/science.html •nssdc.gsfc.nasa.gov/planetary/text/mathilde.txt •neo.jpl.nasa.gov/images/mathilde.html
VESTA	•aa.usno.navy.mil/ephemerides/asteroid/masses /PressRelease.htm

circumstances DS1 was the first s/c, which has succeeded in measuring the magnetic field of an asteroid directly.

Considering the magnetic quantities of the other selected asteroids in comparison to Braille, a solid conformity between them and the measurements at Braille is evident. The magnetic properties of Braille have been derived directly from the flyby magnetic field data. The magnetic moment of Gaspra was taken from *Kivelson et al.* [1994] and the remaining magnetic quantities were calculated from this moment. For the other asteroids estimations of the magnetic quantities are just based on the material properties as there were no flyby data available; therefore, the results have been put in brackets. It will be very exciting to analyze the magnetic field data of the NEAR s/c orbiting around the asteroid EROS. Until now, however, where the NEAR orbits at an altitude of 15 km, no significant magnetic structures are visible [*Acuña*, 2000].

Conclusion

Concluding these investigations, it can be stated that in spite of the strong magnetic disturbances of DS1 successful magnetic field measurements at the asteroid Braille could be performed, which led to an estimate of an upper limit of its magnetic moment in the order of $2.1 \cdot 10^{11}\,\mathrm{Am}^2$. Comparison of characteristic quantities of Braille with other asteroids showed good conformity. We are looking forward to the flyby of DS1 at the comet 19P/Borelly in September 2001 and expect interesting new magnetic field data.

Acknowledgments. The work of K.-H. Glassmeier, F. Kuhnke, G. Musmann, C. Othmer, and I. Richter was financially supported by the German Bundesministerium für Bildung und Forschung and the Deutsches Zentrum für Luft- und Raumfahrt under contract 50 OO 99037. Support by the Institute for Computer and Communication Network Engineering (Braunschweig) and the Institute for Space Research (Graz, Austria) is gratefully acknowledged. We thank K. Mehlem (ESTEC) and P.Weidelt (IGM) for supplying the Multi Dipole Model software to fit the dipole of Braille. We express our thanks to M. Acuña (GSFC) for fruitful conversations.

References

Acuña, M., NEAR Magnetic field observations at 433 EROS: First results (Abstract), 33rd COSPAR Scientific Assembly, Warsaw, July 2000.

Baumgärtel, K., K. Sauer, A. Bogdanov, A Magnetospheric Model of Solar Wind Interaction with Asteroid Gaspra, *Science, Vol. 263*, pp. 653–655, Feb. 1994.

Baumgärtel, K., K. Sauer, T. R. Story, Solar Wind Response to a Magnetized Asteroid: Linear Theory, *Icarus, 129*, pp. 94-105, 1997.

Brinza, D. E., et al., Ion Propulsion Subsystem Environmental Effects on Deep Space 1: Initial Results from the IPS Diagnostic Subsystem, DS1 Technology Validation Report, *JPL Pub., 00-10(4b)*, 2000.

Chatfield, C., A.J. Collins, *Introduction to multivariate analysis*, Chapman/Hall, New York, London, 1980.

DS 1 Asteroid Flyby, Press Kit, NASA, July 1999.

Glassmeier, K.–H., MAG–RPC: The Fluxgate MAGnetometer in the ROSETTA Plasma Consortium, *ESA–Special Publication SP–1165*, in press, 2001.

Greenstadt, E., Conditions for Magnetic Interaction of Asteroids with the Solar Wind, *Icarus, 14*, pp. 374-381, 1971.

Hicks, M. D., et al., The Deep Space 1 Mission Target 1992 KD: A Connection to Stony Meteorites?, 30th Annual Lunar and Planet. Sci. Conference, Abstract no. 1719, 1999.

Holmes, P., J. L. Lumley, G. Berkooz, *Turbulence, Coherent Structures, Dynamical Systems and Symmetry*, Cambridge Monographs on Mechanics, Cambridge, 1996.

Kivelson, M. G., et al., Magnetic Field Signatures Near Galileo's Closest Approach to Gaspra, *Science, 261*, pp 331–334, 1993.

L. Soderblom et al., Deep Space 1 MICAS Observations of 9969 Braille, American Astronomical Society,*DPS, Abstract No. 3403*, 1999.

I. Richter, K.–H. Glassmeier, F. Kuhnke, G. Musmann, C. Othmer, Institute for Geophysics and Meteorology, Technical University of Braunschweig, Mendelssohnstr. 3, 38106 Braunschweig, Germany. (e-mail: i.richter@tu-bs.de; kh.glassmeier @tu-bs.de; f.kuhnke@tu-bs.de; g.musmann@tu-bs.de; c.othmer @tu-bs.de)

D. E. Brinza, B. T. Tsurutani, Jet Propulsion Laboratory, California Institute of Technology, Pasadena, California 91109. (e-mail: david.e.brinza@jpl.nasa.gov; btsurutani @jplsp3.jpl.nasa.gov)

M. Cassel, Institute for Computer and Communication Network Engineering, Technical University of Braunschweig, Hans-Sommer-Str. 66, 38106 Braunschweig, Germany. (e-mail: cassel@ida.ing.tu-bs.de)

K. Schwingenschuh, Institute for Space Research, Technical University of Graz, Schmiedelstr. 6, 8042 Graz, Austria. (e-mail: konrad.schwingenschuh@oeaw.ac.at)

(Received November 24, 2000; revised January 18, 2001; accepted February 9, 2001.)

Proceedings of ISSS-6 (2001): 1–4

ISSS–6

Parallel PIC-code simulations of ion thruster-induced plasma dynamics

C. Othmer[1], **K.-H. Glassmeier**[1], **U. Motschmann**[2], **and J. Schüle**[3]

[1]Institut für Geophysik und Meteorologie, TU Braunschweig, Germany
[2]Institut für Theoretische Physik, TU Braunschweig, Germany
[3]Rechenzentrum der TU Braunschweig, Germany

Abstract. Recently, there is a strong interest in ion thrusters as propulsion devices for interplanetary missions. The operation of such thrusters in space induces a very dynamic plasma environment. A proper understanding of this environment is a prerequisite for the interpretation of scientific measurements aboard ion-propelled spacecrafts, as in the case of the Deep Space 1 asteroid and comet flybys (Richter et al., 2001). We give an overview of the thruster-induced plasma environment and describe the numerical simulation with which we attempt to explore its main dynamical phenomena. Special emphasis is paid to the particle injection scheme, which allows a self-consistent injection of non-neutral plasmas with charge-conserving local electromagnetic field solvers, and to the taskfarm-based parallelization of the code.

1 The ion thruster-induced plasma environment

Electric propulsion devices are regarded as the next-generation type of space propulsion for interplanetary missions. Recently, interest in such devices has grown considerably: NASA's Deep Space 1 (DS1) spacecraft, which is currently on its way to encounter comet Borelli, is equipped with an ion thruster, and the European Space Agency is planning to employ an electric propulsion engine on its SMART-1 mission to the moon.

Figure 1 shows a photograph of the ion thruster that operates aboard Deep Space 1. It has a diameter of about 40 cm and, as every ion engine, it derives its thrust from the electrostatic acceleration of heavy ions. Outside the thruster, the ejected ions form a dense beam with a characteristic kinetic energy of about 1 keV. The maximum thrust thereby achieved amounts to 90 mN.

In order for the ion beam to propagate, it needs to be electrically neutralized. For this purpose, a hollow cathode is mounted on the thruster periphery that injects electrons into the beam. The electrostatic forces between electrons and ions are thought to induce a mixing between these two species and to generate a quasi-neutral plasma beam. Recombination is negligible in the neutralization process due to its small effective cross section. Apart from that, some unionized neutrals escape from the thruster and – through collisions with energetic beam ions – generate a low-energy charge-exchange plasma plume around the thruster (CEX).

Hence, an ion thruster produces a very dynamic plasma environment. Three different plasma regimes can be identified: (1) the CEX plasma plume around the spacecraft, (2) the neutralization, i. e. the mixing between the beam ions and the electrons ejected by the hollow cathode, and (3) the interaction of the neutralized thruster beam with the ambient solar wind.

While the dynamics of CEX ions have been the subject of extensive theoretical studies (Wang and Brophy, 1995; Samanta Roy et al., 1996a, 1996b; Wang et al., 1996) and some experimental verifications (de Boer, 1997; Wang et al., 2000), the neutralization process and the solar wind-thruster beam interaction have received only minor attention. The thoroughest treatments of ion thruster beam neutralization date back to as early as the 1960's. Buneman and Kooyers (1963), Dunn and Ho (1963), and Wadhwa et al. (1965) carried out one- and two-dimensional computer simulations of the mixing between cold streaming ions and cold or hot

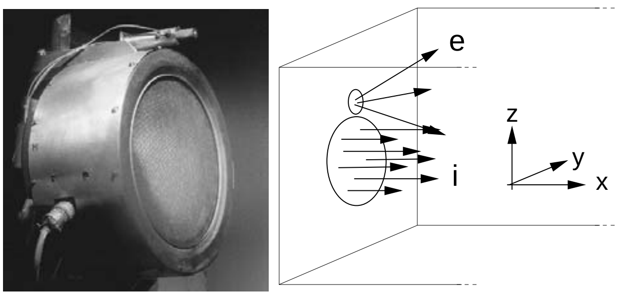

Fig. 1. Photograph of the DS1 ion thruster (note the hollow cathode-neutralizer attached at the top) and our simulation geometry.

Correspondence to: C. Othmer (c.othmer@tu-bs.de)

electrons. These authors found that self-excited fluctuating space-charge fields at the electron plasma frequency provide the mixing of electrons and ions, and lead to the creation of a stably streaming plasma.

Given the very limited computational possibilities by that time, these investigations were primarily aimed at a 'proof of principle' of ion beam neutralization via electron injection, rather than dedicated to an in-depth study of the plasma physical processes that accompany the neutralization.

The question of interaction between the quasi-neutral beam plasma and the ambient solar wind has not been considered at all. It differs considerably from other beam-plasma scenarios in that the high-density beam has a lateral scale of just several decimeters, which is much less than typical scale lengths of the solar wind. While the thruster beam will pass rather unaffected through the teneous solar wind due to the huge density contrast between the beam and the solar wind (roughly $4 \cdot 10^9$, Othmer et al., 2000), it might, however, drive instabilities in the solar wind plasma.

Aiming at studying the neutralization regime as well as the thruster beam interaction with the solar wind, we have developed a parallel 3D electromagnetic particle-in-cell (PIC) code. The code will be described in the following with special emphasis paid to the particle injection scheme and the parallelization.

2 The numerical model

We intend to investigate both the thruster beam neutralization regime and the possible interaction of the neutralized ion beam with the ambient solar wind. The distinct characters of these two plasma scenarios had to be taken into account for the design of the numerical model. The neutralization, i. e. the mixing between initially spatially separated electrons and ions involves a highly non-neutral plasma and is obviously dominated by electrostatic forces. Once the beam is neutralized, however, the electrostatic forces become less important, and electromagnetic phenomena such as the self-consistently generated magnetic field of the beam particles might play a role for the possible interaction of the beam with the solar wind. Even for a 99% neutralized ion beam this magnetic field amounts to about 25 nT in the case of DS1 (Othmer et al., 2001a), as compared to the 5 nT of the solar wind at 1 AU. Hence, a proper description of both plasma scenarios requires a fully electromagnetic simulation model, which is, moreover, capable of dealing with highly non-neutral plasmas.

The simulation we developed is a parallel three-dimensional electromagnetic particle-in-cell code, which runs on any parallel computer where the Message-Passing-Interface (MPI, 1994; MPI-2, 1997) is installed. The basic algorithms are similar to those of Buneman's TRISTAN code (Buneman, 1993): Electrons and ions are pushed using a standard relativistic leapfrog push algorithm (Birdsall and Langdon, 1985), and the currents that arise from the particle movements are calculated via a rigorous charge conservation scheme (Villasenor and Buneman, 1992). The electric and magnetic fields are defined on a spatially staggered 3D cartesian grid (Yee, 1966). They are obtained self-consistently by leapfrogging in time and central differencing Maxwell's two curl-equations

$$\frac{\partial \mathbf{B}}{\partial t} = -\nabla \times \mathbf{E} \quad \text{and} \quad \frac{1}{c^2}\frac{\partial \mathbf{E}}{\partial t} = \nabla \times \mathbf{B} - \mu_0 \mathbf{j}\,. \tag{1}$$

The second pair of Maxwell's equations,

$$\nabla \cdot \mathbf{B} = 0 \quad \text{and} \quad \nabla \cdot \mathbf{E} = \rho\,, \tag{2}$$

do not have to be solved in our code. They are fulfilled identically because (a) $\mathbf{B}$ is updated via Eq. (1), and (b) by virtue of the charge-conserving character of the current assignment scheme (cf. Villasenor and Buneman, 1992).

We simulate the region downstream of the thruster exit. In order to reproduce the actual ion thruster geometry, electrons and ions are injected as depicted in Fig. 1. Both species enter the simulation box in same numbers per time step through a round opening, with the electrons' opening being smaller and attached to the top of the ions'.

2.1 Particle injection

A consequence of employing a rigorously charge-conserving local field solver is that the charge density ρ does not appear explicitly, so that particles give rise to electric fields not via their charges but only by virtue of the currents they produce. This has to be taken into account for the injection of new and the removal of leaving particles. Suppose that a particle of charge $+q$ is "injected" into vacuum at $\mathbf{x}_0$ with a velocity $\mathbf{v}$, moves to $\mathbf{x}_1 = \mathbf{x}_0 + \mathbf{v}\Delta t$ after one timestep and is forced to stay there. As a consequence of charge conservation, the electric field that will develop from such a configuration is not a monopole Coulomb-field corresponding to the positive charge at $\mathbf{x}_1$, but a dipole field caused by $+q$ at $\mathbf{x}_1$ and a virtual negative charge $-q$ at $\mathbf{x}_0$.

A cure for these unwanted virtual charges or, in other words, for artificial divergences of $\mathbf{E}$ is to generate particles in pairs of oppositely signed charges that are injected at the same location $\mathbf{x}_0$ (Buneman, 1993). However, due to the creation of charges in pairs, it can only be applied as long as the plasma to be injected is quasi-neutral. It does not work in situations that require the injection of non-neutral plasmas. That is why for our simulation of ion thrusters with their spatially separated electron and ion sources, a new injection scheme had to be developed, which respects conservation of charge (Othmer et al., 2001b). This scheme consists of a kind of electrical "generator" that creates the particles in pairs of oppositely signed charges at the same location, moves them to their respective injection positions and finally releases them with their actual injection velocities. It suppresses the emergence of artificial divergences of $\mathbf{E}$ completely and allows a self-consistent injection of non-neutral plasmas with rigorously charge-conserving local electromagnetic field solvers.

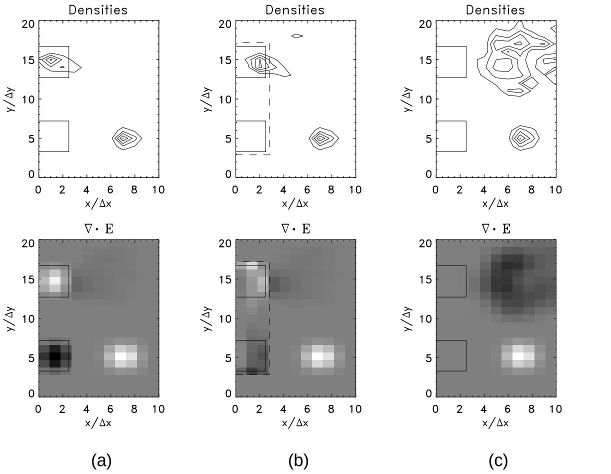

Fig. 2. Snapshots of three sample simulations with different particle injection schemes. Electrons and ions are generated in the top and bottom rectangles, respectively, adjacent to the left border. Their injection bulk velocities are $v_x = 0.1c$, and the electron thermal velocity is $0.01c$. The ion mass was chosen to be that of Xenon ions, i. e. 250,000m_e, and the ions have a negligible thermal spread corresponding to $T_i = T_e$. *Top panels:* electron and ion densities. *Bottom panels:* divergence of the electric field. Black and white correspond to negative and positive divergence, respectively. The background grey tone indicates zero divergence. (a) No compensation, (b) with an electrically conductive region within the dashed rectangle, (c) using our "generator technique". Note the emergence of virtual charges within the particle injection areas in (a) and (b). When employing the generator (c), the electric field in the injection regions is divergenceless and the electrons can expand freely (modified after Othmer et al., 2001b)

Fig. 2 shows the effect of the generator for sample simulations with spatially separated electron and ion sources. In contrast to injecting the particles without any correction to the electric field (a) or applying a finite electric conductivity in the injection region (b), the generator-based injection (c) leads to a divergenceless electric field in the injection area.

2.2 Parallelization

Being a 3D PIC-simulation, our code has high requirements towards computational power and had to be implemented on a parallel computer. In general, for running efficiently in parallel, the total workload associated with the simulation has to be distributed as equally as possible among the various processors (PEs – processing elements). This is usually done by dividing the physical simulation volume into a set of equally-sized sub-volumes ("domains") each of which is assigned to one PE. Every PE is then responsible for the field and particle update within its domain (e. g. Wang et al., 1995).

As long as the particle distribution over the simulation volume is roughly homogeneous, such a domain decomposition generates the same workload on every PE. In our simulations of ion thruster beam neutralization, however, the particles are injected in a spatially very localized region and their distribution over the simulation volume is highly inhomogeneous. PEs, whose domains are very close to or even include the particle beam, are responsible for considerably more particles than those farther off, which might not even get a single particle throughout the whole simulation. This inhomogeneity in the particle distribution causes a strong imbalance of workload and thus leads to a poor parallel efficiency.

In order to better balance the particle work in such cases, Liewer and Decyk (1989) suggested to introduce a *secondary* decomposition that adjusts itself dynamically to accomodate roughly the same number of particles in each domain. The secondary decomposition is also a physical division of the simulation box into sub-volumes, but it is independent of the primary equidistant decomposition and is only determined by the current particle distribution.

Named "General Concurrent Particle-in Cell" algorithm (GCPIC), Liewer and Decyk's dynamic load balancing with two independent decompositions clearly generates the same amount of particle and grid work on every PE. Its drawback is, however, that it does not preserve data locality and thus involves a great deal of inter-processor communication: With only a single decomposition every PE has all the data at its disposal that is needed to update particles and fields. An exchange of particle or field data is necessary only at the domain boundaries (via ghost cells, e. g. Wang et al., 1995). This changes dramatically for the GCPIC. In order to update the particles in its particle domain, a PE has to gather all the field data of the corresponding region of the simulation box from the various PEs whose primary domains intersect with this region. Similarly, after calculating the current from the particle movement, it has to send appropriate portions of the total current array to these PEs.

Liewer and Decyk (1989), Ferraro et al. (1993), Lyster et al. (1995), and Wang et al. (1995) implemented the GCPIC into electrostatic and electromagnetic PIC simulations. They found that due to the communication overhead, the dynamic load balancing is counterproductive compared to a single static equidistant decomposition, unless the particle work greatly dominates over the grid work. In his 3D electromagnetic simulations, where the particle push was about 100 times more expensive than the field solver, Wang et al. (1995) achieved a parallel efficiency of nearly 100% by using the GCPIC. The benchmarking of Ferraro et al. (1993), however, who used a code with a ratio between particle work and grid work of about 3, showed the GCPIC to be actually inferior to a static equidistant decomposition.

For some reference simulations with our code, the computational cost of the particle associated work dominated over the grid work by a factor of about 4. Hence, the GCPIC approach will probably not significantly improve the parallel efficiency in our case, and another way of removing the strong imbalance of the particle workload has to be envisaged.

A more promising option than the GCPIC is to implement a so-called "taskfarm": The single static equidistant decomposition is kept, but additionally, on every PE, all the particles are now organized into a certain number of smaller groups each of which forms one "task". Once it is time to push the particles, these groups are traded among *all* PEs. Whenever a PE has finished the work on its own particles, it grabs a particle group of another PE, processes them and writes them back. Hence, PEs with less particles take over parts of the work of other, busier PEs.

The transfer of particle groups from and to their host PE has to happen without the host PE's involvement in order not to hold it off from its own work. Such a "one-sided communication", as it is called in the MPI jargon, which allows one PE to freely access the memory of another, is available in the extension of the MPI standard (MPI-2, 1997).

In order to manage the taskfarm, one of the PEs is assigned the additional duty of being the "taskmaster": It keeps a list of all the tasks, coordinates the work progress and makes sure that no PE is released before all tasks are done.

A taskfarm of this kind – without a taskmaster, though – has been employed e. g. by Carretti (1998) in his simulation of gravitating galaxy clusters. In plasma PIC simulations, however, the taskfarm concept has not been introduced so far. In our talk, we will show how this concept can be implemented in plasma simulations and how it performs as compared to static equidistant domain decompositions.

Acknowledgements. We gratefully acknowledge fruitful discussions with G. Pringle from the Edinburgh Parallel Computing Centre and Ch. Frick from the Rechenzentrum der TU Braunschweig. The work was financially supported by the European Community – Access to Research Infrastructure action of the Improving Human Potential Programme (contract no. HPRI-1999-CT00026) and by the Deutsches Zentrum für Luft- und Raumfahrt under contract no. 50 OO 0102.

References

Birdsall, C. K. and A. B. Langdon, Plasma Physics via Computer Simulation, McGraw-Hill, New York, 1985.

Buneman, O., TRISTAN: The 3-D E-M Particle Code, in: Matsumoto, H., and Y. Omura (Eds.), Computer Space Plasma Physics, Terrapub, Tokyo, p. 67, 1993.

Buneman, O., and G. Kooyers, Computer simulation of the electron mixing mechanism in ion propulsion, AIAA-Journal, 1, 2525, 1963.

Carretti, E., Numerical simulations and power spectrum analysis of ESP redshift survey, PhD thesis, Università degli Studi di Bologna, Italy, 1998.

de Boer, P. C. T., Measurements of electron density in the charge exchange plasma of an ion thruster, J. Propulsion and Power, 13, 783, 1997.

Dunn, D. A., and I. T. Ho, Computer experiments on ion beam neutralization with initially cold electrons, AIAA-Journal, 1, 2770, 1963.

Ferraro, R. D., P. C. Liewer, and V. K. Decyk, Dynamic load balancing for a 2D concurrent plasma PIC code, J. Comput. Phys., 109, 329, 1993.

Liewer, P. C., and V. K. Decyk, A general concurrent algorithm for plasma particle-in-cell simulation codes, J. Comput. Phys., 85, 302, 1989.

Lyster, P. M., P. C. Liewer, V. K. Decyk, and R. D. Ferraro, Implementation and characterization of three-dimensional particle-in-cell codes on multiple-instruction-multiple-data massively parallel supercomputers, Computers in Physics, 9 (4), 420, 1995.

MPI, A Message-Passing Interface Standard, Message Passing Interface Forum, http://www.mpi-forum.org, 1994.

MPI-2, Extensions to the Message-Passing Interface, Message Passing Interface Forum, http://www.mpi-forum.org, 1997.

Othmer, C., K. H. Glassmeier, U. Motschmann, J. Schüle, and Ch. Frick, Three-dimensional simulations of ion thruster beam neutralization, Phys. Plas., 7 (12), 5242, 2000.

Othmer, C., K. H. Glassmeier, U. Motschmann, J. Schüle, and Ch. Frick, Numerical Simulations of Ion Thruster-induced Plasma Dynamics – The Model an Initial Results, Adv. Space Res., submitted, 2001a.

Othmer, C., U. Motschmann, and K. H. Glassmeier, Creation of spatial charge separation in plasmas with rigorously charge-conserving local electromagnetic field solvers, J. Comput. Phys., submitted, 2001b.

Richter, I., D. E. Brinza, M. Cassel, K. H. Glassmeier, F. Kuhnke, G. Musmann, C. Othmer, K. Schwingenschuh, B. T. Tsurutani, First Direct Magnetic Field Measurements of an Asteroidal Magnetic Field: DS1 at Braille, Geophys. Res. Lett., 28 (10), 1913, 2001.

Samanta Roy, R., D. Hastings, and N. Gatsonis, Ion-thruster modeling for backflow contamination, J. Spacecraft and Rockets, 33 (4), 525, 1996a.

Samanta Roy, R., D. Hastings, and N. Gatsonis, Numerical study of spacecraft contamination and interaction by ion-thruster effluents, J. Spacecraft and Rockets, 33(4), 535, 1996b.

Villasenor, J., and O. Buneman, Rigorous charge conservation for local electromagnetic field solvers, Comp. Phys. Comm., 69, 306, 1992.

Wang, J., and J. Brophy, 3-D Monte-Carlo particle-in-cell simulations of ion thruster plasma interactions, AIAA 95-2826, 1995.

Wang, J., P. Liewer, and V. Decyk, 3D electromagnetic plasma particle simulations on a MIMD parallel computer, Comp. Phys. Comm., 87, 35, 1995.

Wang, J., J. Brophy, and D. Brinza, 3-D simulations of NSTAR ion thruster plasma environment, AIAA 96-3202, 1996.

Wang, J., D. E. Brinza, D. T. Young, J. E. Nordholt, J. E. Polk, M. D. Henry, R. Goldstein, J. J. Henly, D. J. Lawrence, and M. Shappirio, Deep Space One investigations of ion propulsion plasma environment: initial results, J. Spacecraft and Rockets, submitted, 2000.

Wadhwa, R. P. , O. Buneman, and D. F. Brauch, Two-dimensional computer experiments on ion-beam neutralization, AIAA-Journal, 3, 1076, 1965.

Yee, K. S., Numerical solution of initial boundary value problems involving Maxwell's equations in isotropic media, IEEE Trans. Ant. Propagat., 14, 302, 1966.

DEEP SPACE 1 - Die Mission

I. Richter, K.-H. Glaßmeier, F. Kuhnke, G. Musmann, C. Othmer

Überblick

DEEP SPACE 1 (DS1) ist die erste NASA-Mission im Rahmen des New Millennium Programms. Sie hat das Ziel, 12 neuartige Technologien für die Raumfahrt des dritten Jahrtausends zu testen. Als wesentliche Punkte sind zu nennen:

- DS1 wird als erstes Raumfahrzeug auf einer Deep Space Mission mit einem Ionentriebwerk angetrieben.
- DS1 ist mit einem autonomen Navigationssystem (AutoNav) ausgestattet.
- DS1 besitzt das neuartige Kamerasystem MICAS (Miniature Integrated Camera Spectrometer) zur Navigation und zur Spektralanalyse. Es ist nur etwa 1 cm^3 groß.
- Die Stromversorgung von DS1 wird durch zwei neuartige Solarpanels mit hocheffektiven Focussierlinsen gesichert (SCARLET: Solar Concentrator Arrays with Refractive Linear Element Technology).
- Die Panels liefern 2.5 kW Leistung in 1 AU Entfernung von der Sonne.
- DS1 hat ein Experiment zur Plasmauntersuchung (PEPE: Plasma Experiment for Planetary Exploration) an Bord.
- DS1 ist mit zwei Fluxgatemagnetometern (FGM) ausgestattet. Sie wurden hier am IGM in Zusammenarbeit mit dem Institut für Datenverarbeitungsanlagen und dem Institut für Weltraumforschung in Graz entwickelt und kalibriert.

.

DS1 wurde am 24. Oktober 1998 am Kennedy Space Flight Center, Cap Canaveral, Florida erfolgreich gestartet. DS1 ist 486 kg schwer und hat 81 kg Xenon Gas für den Ionenantrieb an Bord.

Das primäre Ziel des Fluges war ein Rendezvous mit dem Asteroiden Braille am 29. Juli 1999. Das Treffen fand bei einer Entfernung von 1.3 AU von der Sonne statt. Die Vorbeiflugdistanz war mit 28 km extrem niedrig. Das zweite erfolgreich erreichte Missionsziel war der nahe Vorbeiflug (in 2150 km Abstand) am Kometen Borrelly am 22. September 2001.

Die DS 1-Trajektorie

Wissenschaftliche Ziele

Während des gesamten Fluges liefert das Fluxgatemagnetometer aufschlußreiche Magnetfelddaten, mit denen die Plasmaumgebung und die Zusammensetzung der umflogenen Asteroiden und Kometen charakterisiert werden können. Im Rahmen der DS1-Mission wird ferner untersucht, in wie weit es mit ionengetriebenen Raumfahrzeugen prinzipiell möglich ist, wissenschaftlich signifikante Magnetfelddaten zu erhalten. Die Problematik hierbei liegt einerseits im Ionenstrom, der ein eigenes Magnetfeld erzeugt und andererseits in den beweglichen Ionenstrahlfocussiermagneten, die ein temperaturabhängiges magnetisches Störfeld aufweisen. Es werden Magnetfeldmodelle kreiert, die all die Satellitenparameter enthalten, um aus den gemessenen Magnetfelddaten die Störkomponenten zu eliminieren.

Der Asteroid Braille

Der Komet Borrelly

Das Magnetometer

Am Institut für Geophysik und Meteorologie wurde ein hochempfindliches Subminiatur-Vektor-Fluxgate-Magnetometer entwickelt. Es ist für die extremen Anforderungen im Weltraum konzipiert worden und läßt sich folgendermaßen charakterisieren:

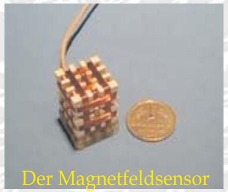

Der Magnetfeldsensor

- Es besitzt eine Auflösung von 0.05 nT bei einem Meßbereich von 25000 nT.
- Es kann in einem Temperaturbereich von -150 °C bis +300 °C operieren.
- Es bestiecht durch eine extrem niedrige Leistungsaufnahme von etwa 200 mW.
- Es kann die 3 Magnetfeldkomponenten mit einer Sampling-Rate von bis zu 20 Vektoren pro Sekunde erfassen.

Der Ionenantrieb

Das Ionentriebwerk

DS 1 gewinnt seinen Schub aus einem solar-elektrischen Ionenantrieb. Der Strom für das Triebwerk wird durch die beiden Solarpanels erzeugt. Als Rückstoßerzeugendes Gas wird das Edelgas Xenon benutzt, das etwa 4.5 mal schwerer als Luft ist. Das Gas wird im Triebwerk durch Stöße ionisiert und im folgenden beim Durchlaufen einer Potentialdifferenz von bis zu 1280 V auf eine Ausstoßgeschwindigkeit von maximal 110000 km/h beschleunigt. Hierbei wird ein Schub von ca. 90 mN erzeugt. Dies entspricht etwa dem Druck, den ein auf der Hand liegendes Blatt Papier ausübt. Dieser Schub ist zwar äußerst gering und würde nie zum Start eines Raumfahrzeuges von der Erde ausreichen; da er aber über Monate (das Xenon reicht für 6000 h Betriebszeit) aufrecht erhalten werden kann und somit für eine kontinuierliche Beschleunigung sorgt, können beachtliche Geschwindigkeiten erreicht werden. DS1 wird nach Verbrauch des gesamten Treibstoffs eine relative Geschwindigkeitserhöhung von 15000 km/h erfahren haben. Bemerkenswert hierbei ist, daß der Ionenantrieb etwa 10 mal mehr Schub liefert als ein konven-tionelles Flüssigkeits- oder Feststofftriebwerk mit gleicher Treibstoffmenge.

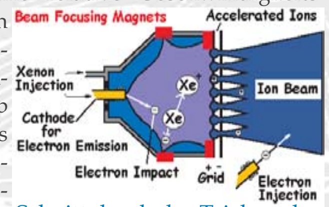

Schnitt durch das Triebwerk

Referenzen

- **First Direct Magnetic Field Measurements of an Asteroidal Magnetic Field: DS 1 at Braille**; I. Richter, D. Brinza, M. Cassel, K.-H. Glassmeier, F. Kuhnke, G. Musmann, C. Othmer, K. Schwingenschuh, B. Tsurutani, Geophys. Res. Lett., Vol. 28, No. 10, 2001
- **Three-dimensional simulations of ion thruster beam neutralization**; C. Othmer, K.-H. Glassmeier, U. Motschmann, J. Schüle, Ch. Frick, Phys. Plas., Vol. 7, No. 12, 2000

DS 1 - Magnetfeldmessungen beim BRAILLE-Vorbeiflug

I. Richter, K.-H. Glaßmeier, F. Kuhnke, G. Musmann, C. Othmer

Überblick

DEEP SPACE 1 (DS 1) hat nach neun Monaten Flugzeit am 29.Juli 1999 ein spektakuläres Rendezvous mit dem Asteroiden BRAILLE (vormals 1992KD) in 1.3 AU Abstand von der Sonne gehabt. Der Closest Approach (CA) fand um 04:46:10 UTC in der extrem geringen Vorbeiflugdistanz von 28 km zum Asteroiden statt. Dabei lieferte das Fluxgate-magnetometer (FGM) hochaufgelöste Magnetfelddaten (20 Hz Meßfrequenz). Die kalibrierten Rohdaten (s. Abbildung) zeichnen sich oberflächlich durch zwei Merkmale aus:

- Es zeigen sich residuale Felder in der Größenordnung von einigen tausend Nanotesla.
- Den Daten sind zahlreiche, etwa 20 nT große Spikes überlagert.

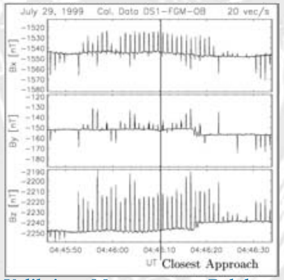

Kalibrierte Magnetometer-Rohdaten des Braille Vorbeiflugs

Die residualen Felder rühren von den Focussiermagneten des Ionentriebwerks her; als Quelle der Spikes sind die magnetischen Kaltgasdüsen für die Fluglageregelung zu nennen.
Um die magnetische Signatur des Asteroiden erkennen zu können, ist daher eine umfangreiches Daten-Processing nötig.

Die Datenanalyse

Aus den Rohdaten werden durch Anwendung der Kalibrierresultate kalibrierte Daten. Nach Drehung in das s/c-System muß der Einfluß der Focussiermagnete berücksichtigt werden. Diese erzeugen ein linear temperaturabhängiges magnetisches Feld, wie die folgenden Plots des evaluierten Temperaturmodells zeigen. Nach dieser Störfeldkorrektur werden die Spikes mit einem geeigneten Kurzzeit-/Langzeitmittel-Spike-Detektor eliminiert.

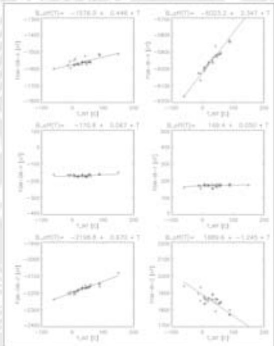

Das Temperaturmodell der Focussiermagnete

Nach der folgenden Mittelung der Daten erhält man den unten gezeigten Plot für die Outboard (OB) und Inboard (IB) Magnetometerdaten.
Auffällig ist, daß sowohl der OB- als auch der IB-Sensor zur Zeit des CA die gleiche Signatur liefern. Dies ist ein Indiz dafür, daß die beobachtete Struktur ihren Ursprung weit außerhalb der Raumsonde hat. Um die Störfelder des Raumfahrzeugs von den externen Sonenwind- und Asteroidenfeldern zu trennen, wird zuguterletzt die Principal Component Analysis (PCA) angewendet. Dies ist eine statistische Methode, die unkorrelierte (interne Felder) von korrelierten (externe Felder) Signalen separiert. Das Resultat für den externen Anteil ist sowohl als diskrete als auch als geglättete Zeitreihe im ganz rechten Datenplot in zeitlich gedehnter Darstellung zu sehen.

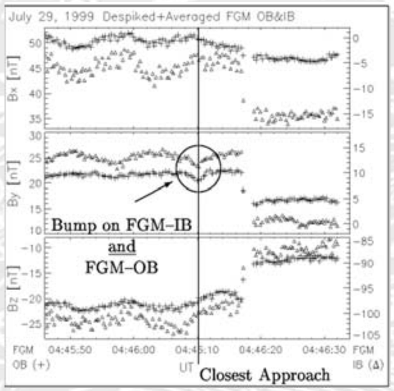

Spike-bereinigte und gemittelte Daten von Outboard und Inboard Magnetometer während des Vorbeiflugs

Das Dipolmodell von BRAILLE

Im folgenden wird versucht, die vorbehandelten Magnetfelddaten als Wirkung eines magnetischen Dipols im Innern des Asteroiden zu deuten. Dazu wird mit der Methode der kleinsten Fehlerquadrate der am besten passende Dipol gesucht.

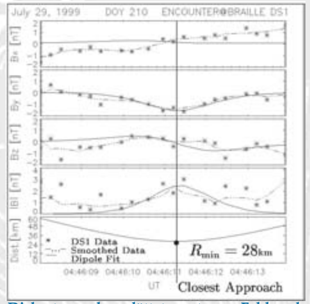

Diskretes und geglättetes externes Feld nach Anwendung der PCA und das gefittete Dipolmodell des Asteroiden BRAILLE

Als Resultat ergibt sich ein zentrischer Dipol mit einem Moment von $2.2 \cdot 10^{11}$ Am^2.

BRAILLE und andere ASTEROIDEN

In der untenstehenden Tabelle wird Braille mit anderen Asteroiden verglichen. Das hier erstmals direkt gemessene Magnetfeld eines Asteroiden und die daraus abgeleiteten Parameter fügen sich gut in die Reihe der anderen ein, so daß ein weiterer Meilenstein zum Verständnis von Asteroiden erreicht werden konnte.

	Vesta	Mathilde	Ida	Eros	Gaspra	Braille
	500 km	60 km	40 km	30 km	25 km	3 km
Dimension [km]		66 X 48x46	59.8 x 25.4 x 18.6	33 x 13 x 13	18.2 x 10.4 x 9.4	2,2 x 1 x 1
Equivalent Radius [km]	265	26	16	9	8.0	0.78
Volume [km^3]	7.80E+07	77000	16100	2600	2145	2
	3900	1340	2600	2700	3900	3900
Material	Basalt,Pyroxene,Olivine	Carbon. Chondrites	Olivine,Orthopyroxene	Pyroxene,Olivine	Metal,Olivine,Pyroxene	Basalt,Pyroxene,Olivine
Spectral Class	S/U-Class	C-Class	S-Class	S-Class	S-Class	Q/S-Class
Mass [kg]	3.04E+20	1.03E+17	4.19E+16	7.02E+15	8.36E+15	7.80E+12
Shape	Sphere	Lump	Croissant	Banana	Potato	Peanut
Periheldistance [AU]	2.15	1.94	2.73	1.13	1.82	1.33
Apheldistance [AU]	2.57	3.35	2.99	1.78	2.59	3.36
Orbital Period [year]	3.63	4.31	4.84	1.76	3.29	3.58
Rotational Period [d]	0.22	17.40	0.19	0.22	0.29	9.4
Encounter		NEAR:27.7.1997	Galileo:28.8.1993	NEAR: 2000	Galileo: 29. 10.1991	DS1: 29.07.1999
Encounter Distance R [km]		1212	2700	100	1600	28
Magnetic Field [nT] @ R		8.6E-01	1.6E-02	5.2E+01	9.8E-03	2
Max. Dipole Moment [Am^2]	7.8E+18	7.7E+15	1.6E+15	2.6E+14	2.0E+14	2.2E+11
Max. Magnetization [A/m]	100	100	100	100	93	110
Max. Surface Field [nT]	83776	83697	83776	84673	78125	92517
Spec. Moment [A m^2 /kg]	0.026	0.075	0.038	0.037	0.024	0.028

DS 1 - Magnetfeldmessungen beim BORRELLY-Vorbeiflug

I. Richter, K.-H. Glaßmeier, F. Kuhnke, G. Musmann, C. Othmer

Überblick

Am 22. September 2001 um 22:29:29 UTC hatte die Raumsonde DS1 ein spektakuläres Rendezvous mit dem Kometen Borrelly. Dabei betrug die minimale Vorbeiflugdistanz nur 2158 km. Das Raumfahrzeug flog in der Ekliptik mit einer relativen Geschwindigkeit von 16.5 km/s am Borrelly vorbei (upstream), wobei der Komet die Ekliptik von Süden nach Norden durchstieß.

Der Komet Borrelly

Borrelly mit Schweif

Der Komet 19P/Borrelly ist ein "bowling pin" förmiger Himmelskörper von etwa 8 km x 4 km Ausdehnung. Zum Zeitpunkt des Rendezvous befand er sich in einem Abstand von 1.36 AU zur Sonne. Mit dem neuartigen Kamerasystem an Board von DS 1 gelang es erstmalig, hochaufgelöste Bilder des Kometen zu erzeugen.

Bereits 6 Stunden vor den Closest Approach (CA) lieferte das Braunschweiger Fluxgate-Magnetometer Magnetfelddaten mit einer zeitlichen Auflösung von 1 s. In einem 40 minütigen Zeitintervall in der Nähe des CA sind sogar hochaufgelöste 20 Hz Daten verfügbar.

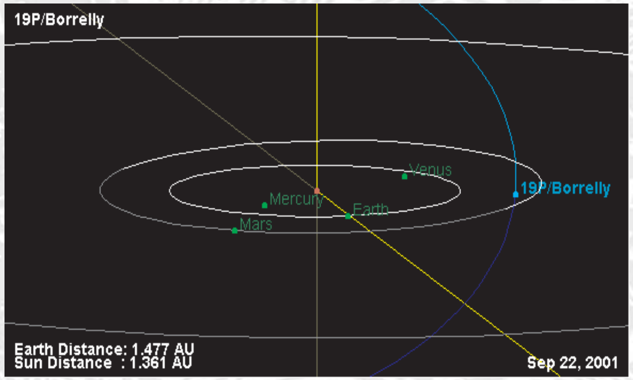

Erste Analyse der Magnetfelddaten in der Umgebung des Kometen Borrelly

In der nebenstehenden Graphik werden prozessierte Magnetfelddaten, die während des Vorbeiflugs am Kometen gemessen wurden, dargestellt. Diese Daten wurden aus den Rohdaten mittels der Ergebnisse der Bodenkalibrierung und dem entwickelten Temperaturmodell der Ionenstrahlfocussiermagnete von DS 1 gewonnen. Des weiteren wurde das Störfeld des Raumfahrzeugs durch eine Hauptkomponentenanalyse (PCA) eliminiert.

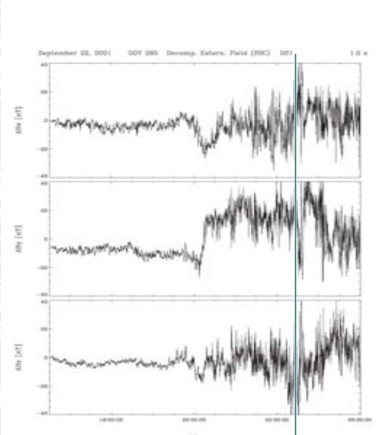

Closest Approach

Besonders auffällig bei diesen Daten ist ein Sprung im Magnetfeld um etwa 20:15, also 2.25 Stunden vor dem Rendezvous (entsprechend etwa 135000 km Entfernung zum Borrelly); ferner ist nach diesem Sprung eine erhöhte Wellenaktivität durch Wechselwirkung mit dem umgebenen Plasma zu erkennen.

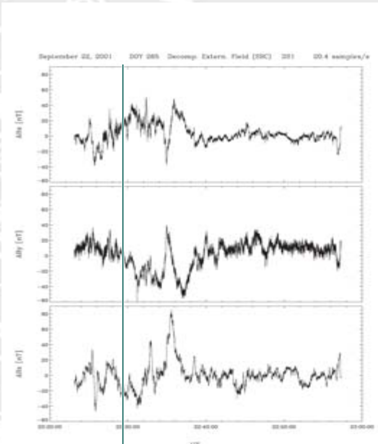

Closest Approach

Die linke Graphik zeigt die hochaufgelösten Daten in unmittelbarer zeitlicher Umgebung des CA. Besonders auffällig hierbei sind Magnetfeldänderungen in der Größenordnung von 100 nT, die sich etwa 6 Minuten nach der dichtesten Annäherung ereigneten. Ähnliche Signaturen wurden bereits bei Vorbeiflügen früherer Missionen an den Kometen Halley, Grigg-Skjellerup und Giacobini-Ziner gesehen.

Eine detailiertere Untersuchung des Kometen kann mittels der Spektralanalyse erreicht werden.

Die rechte Abbildung zeigt das dynamische Spektrum der Magnetfelddaten. Deutlich ist die erhöhte Wellenaktivität in der Nähe des Kometen zu erkennen. Noch signifikanter sind die Spektrallinien im trendbereinigten, linearen Spektrum der unteren Graphik. Es repräsentiert die Frequenzverteilung zum Zeitpunkt des Rendezvous.

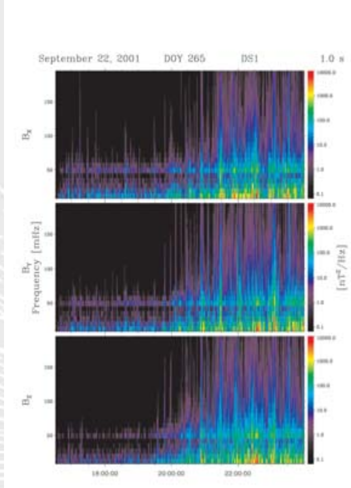

Dynamisches Magnetfeldspektrum: In der Nähe des Kometen ist erhöhte Turbulenz zu verzeichnen.

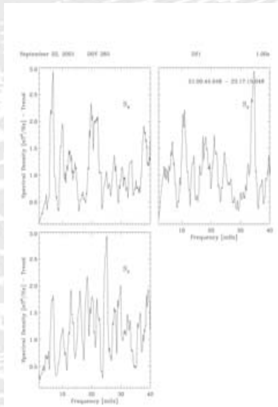

Trendbereinigtes Spektrum: Die Spektrallinien versprechen Rückschlüsse auf die chemische Zusammensetzung.

Durch Vergleich der gemessenen Spektrallinien mit den theoretischen Gyrofrequenzen potentieller Ionen im Plasma lassen sich bei bekanntem Hintergrundmagnetfeld möglicherweise Rückschlüsse auf die chemische Zusammensetzung der Plasmaumgebung ziehen.

Ausblick

Mit dem DS 1 Vorbeiflug am Kometen Borrelly wurde ein weiterer Meilenstein in der Kometenphysik erreicht. Die weitergehende Analyse der gemessenen Daten verspricht, die Kenntnisse über Kometen zu vertiefen.

DS1 - Ion thruster-induced plasma dynamics

C. Othmer (IGM), K.-H. Glaßmeier (IGM), U. Motschmann (IThP), J. Schüle (RZ)

The thruster-induced plasma environment

Ion thrusters are regarded as the next-generation type of space propulsion. Their mass efficiency makes them superior to conventional chemical propulsion systems, especially on long-term missions like Deep Space 1. However, the dynamic plasma environment induced by ion thrusters has raised various concerns in terms of its potential impact on the spacecraft and on scientific instruments aboard. Our studies address two aspects of this

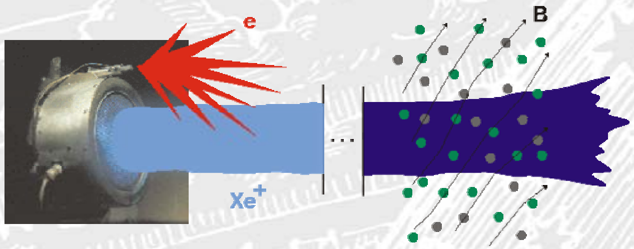

environment: (1) the neutralization regime, i.e. the mixing between beam ions and electrons ejected by the hollow-cathode neutralizer and (2) the interaction of the neutralized thruster beam with the ambient solar wind. In close cooperation with the Institute of Theoretical Physics (IThP) and the University's Rechenzentrum (RZ) we investigate these two plasma regimes by means of a numerical simulation.

The numerical model: ISOLDE

Our simulation is a 3D electromagnetic Particle-in-cell code. Both electrons and xenon ions are treated as particles, which enter the simulation volume from one side. The code is capable of modelling electrostatic as well as electromagnetic phenomena by integrating Maxwell's equations on a spatially staggered grid. By means of a "taskfarm" strategy for the dynamic balancing of the workload, it runs with high parallel efficiency on the CRAY T3Es of the Institute of Scientific Computing (Braunschweig) and the Edinburgh Parallel Computing Centre. In order to inject electrons and ions self-consistently through spatially separated sources, we have developed a "generator" that makes the code well-suited for the simulation of ion thrusters: ISOLDE, the **I**on engine **Sol**ver.

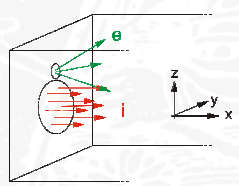

Shock-Neutralization

At the present stage of our investigations, we have applied ISOLDE to the neutralization regime of an ion thruster: the electrons are injected with a thermal velocity distribution and the ions with a uniform bulk velocity plus a negligible thermal spread. As a first step towards understanding the complex process of thruster beam neutralization, we simplified the injection geometry by disregarding the spatial separation between the electron and the ion source.

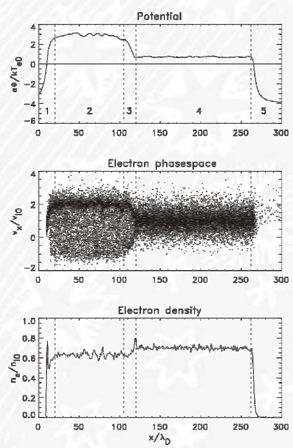

The most remarkable result of our simulation runs in this quasi-1D geometry is the dominant role of the injection velocity ratio η between electron thermal velocity and ion bulk velocity. Depending on the value of η, the overall beam behaviour switches between two completely different scenarios. For η being smaller than 1.7, a moving electrostatic shock front emerges, which generates a fully thermalized plasma, whereas for larger η no such shock occurs and the plasma does not become thermalized.

Shock-Neutralization for η=1: The particles are injected at x=10 and have moved up to x=260. Note the potential drop, the density jump and the dramatic change in the electron phase space across the shock front around x=110.

As today's ion thrusters operate at η-values between 10 and 20, the shock-neutralization has not been reported so far. For the design of future thrusters, however, it represents a promising option: thrusters undergoing shock-neutralization would generate a thermalized beam plasma with no free energy to drive unwanted plasma instabilities and hence less electromagnetic interference.

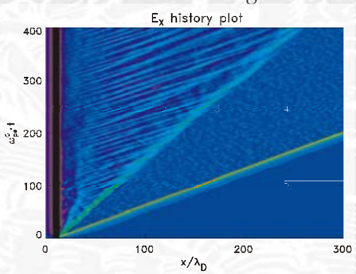

The axial electric field for η=1: Note the injection sheath (1), the beam-plasma unstable waves (2), the moving shock front (3), the region of thermalized plasma (4) and the vacuum ahead of the beam (5).

Separated particle sources

For an injection geometry with spatially separated particle sources, we investigated the shock-free neutralization regime. Also in this configuration, the velocity ratio η continues to control the electron dynamics.

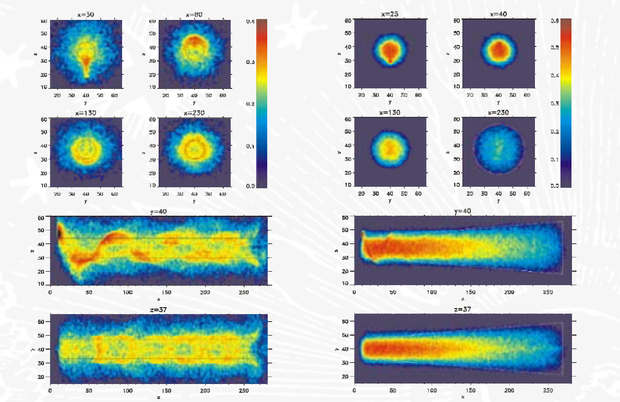

Electron density distribution in several cuts through the simulation volume for η=1 (left) and η=8 (right). The density is normalized to the nominal ion density of a non-diverging beam. Note the meandering movement of the electrons, which dominates their dynamics for η=1 and is still present for η=8.

In order to quantify the impact of η, we derived scaling laws for some basic plasma parameters of the neutralized beam, such as degree of non-neutrality, wavelength of the meandering electron movement, electron temperature and beam potential. In combination with the measurements aboard Deep Space 1, these laws give a coherent picture of the impact of η on the neutralization process.

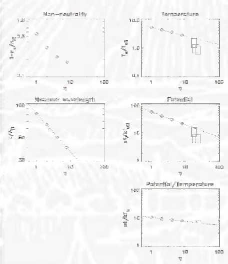

Dependence of various beam parameters on η: simulation results (diamonds) and measurements aboard Deep Space 1 (boxes, after Wang et al., 2001).

References

Othmer, C., K.H. Glassmeier, U. Motschmann, J. Schüle, and Ch. Frick, Three-dimensional simulations of ion thruster beam neutralization, *Phys. Plas.*, **7** (12), 5242, 2000.

Wang, J., et al., DS1 investigations of ion propulsion plasma environment: initial results, *J. Spacecr. Rockets*, subm., 2001.

DS1 - Ion thruster-induced plasma dynamics

C. Othmer (IGM), K.-H. Glaßmeier (IGM), U. Motschmann (IThP), J. Schüle (RZ)

The thruster-induced plasma environment

Ion thrusters are regarded as the next-generation type of space propulsion. Their mass efficiency makes them superior to conventional chemical propulsion systems, especially on long-term missions like Deep Space 1. However, the dynamic plasma environment induced by ion thrusters has raised various concerns in terms of its potential impact on the spacecraft and on scientific instruments aboard. Our studies address two aspects of this

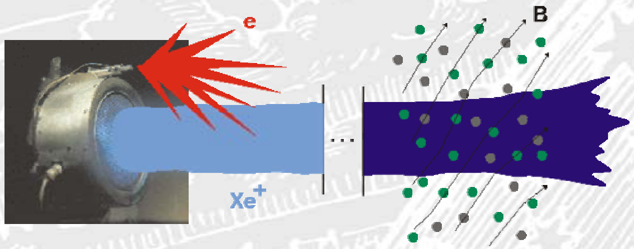

environment: (1) the neutralization regime, i.e. the mixing between beam ions and electrons ejected by the hollow-cathode neutralizer and (2) the interaction of the neutralized thruster beam with the ambient solar wind. In close cooperation with the Institute of Theoretical Physics (IThP) and the University's Rechenzentrum (RZ) we investigate these two plasma regimes by means of a numerical simulation.

The numerical model: ISOLDE

Our simulation is a 3D electromagnetic Particle-in-cell code. Both electrons and xenon ions are treated as particles, which enter the simulation volume from one side. The code is capable of modelling electrostatic as well as electromagnetic phenomena by integrating Maxwell's equations on a spatially staggered grid. By means of a "taskfarm" strategy for the dynamic balancing of the workload, it runs with high parallel efficiency on the CRAY T3Es of the Institute of Scientific Computing (Braunschweig) and the Edinburgh Parallel Computing Centre. In order to inject electrons and ions self-consistently through spatially separated sources, we have developed a "generator" that makes the code well-suited for the simulation of ion thrusters: ISOLDE, the **I**on engine **Sol**ver.

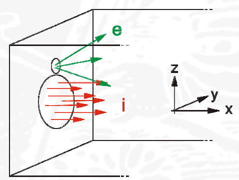

Shock-Neutralization

At the present stage of our investigations, we have applied ISOLDE to the neutralization regime of an ion thruster: the electrons are injected with a thermal velocity distribution and the ions with a uniform bulk velocity plus a negligible thermal spread. As a first step towards understanding the complex process of thruster beam neutralization, we simplified the injection geometry by disregarding the spatial separation between the electron and the ion source.

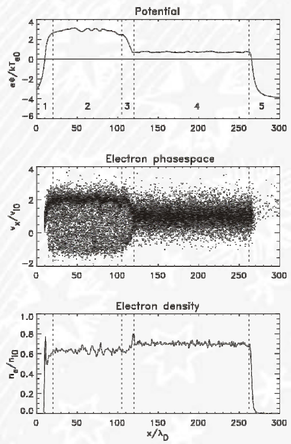

The most remarkable result of our simulation runs in this quasi-1D geometry is the dominant role of the injection velocity ratio η between electron thermal velocity and ion bulk velocity. Depending on the value of η, the overall beam behaviour switches between two completely different scenarios. For η being smaller than 1.7, a moving electrostatic shock front emerges, which generates a fully thermalized plasma, whereas for larger η no such shock occurs and the plasma does not become thermalized.

Shock-Neutralization for η=1: The particles are injected at x=10 and have moved up to x=260. Note the potential drop, the density jump and the dramatic change in the electron phase space across the shock front around x=110.

As today's ion thrusters operate at η-values between 10 and 20, the shock-neutralization has not been reported so far. For the design of future thrusters, however, it represents a promising option: thrusters undergoing shock-neutralization would generate a thermalized beam plasma with no free energy to drive unwanted plasma instabilities and hence less electromagnetic interference.

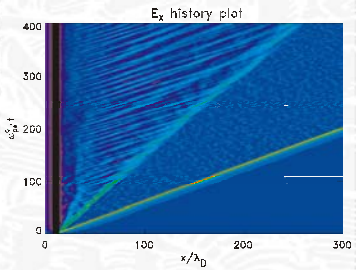

The axial electric field for η=1: Note the injection sheath (1), the beam-plasma unstable waves (2), the moving shock front (3), the region of thermalized plasma (4) and the vacuum ahead of the beam (5).

Separated particle sources

For an injection geometry with spatially separated particle sources, we investigated the shock-free neutralization regime. Also in this configuration, the velocity ratio η continues to control the electron dynamics.

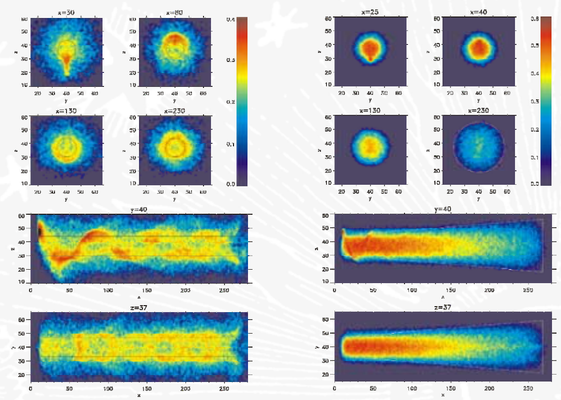

Electron density distribution in several cuts through the simulation volume for η=1 (left) and η=8 (right). The density is normalized to the nominal ion density of a non-diverging beam. Note the meandering movement of the electrons, which dominates their dynamics for η=1 and is still present for η=8.

In order to quantify the impact of η, we derived scaling laws for some basic plasma parameters of the neutralized beam, such as degree of non-neutrality, wavelength of the meandering electron movement, electron temperature and beam potential. In combination with the measurements aboard Deep Space 1, these laws give a coherent picture of the impact of η on the neutralization process.

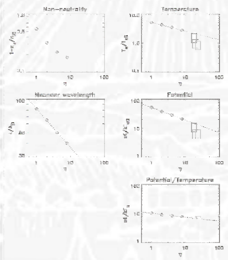

Dependence of various beam parameters on η: simulation results (diamonds) and measurements aboard Deep Space 1 (boxes, after Wang et al., 2001).

References

Othmer, C., K.H. Glassmeier, U. Motschmann, J. Schüle, and Ch. Frick, Three-dimensional simulations of ion thruster beam neutralization, *Phys. Plas.*, **7** (12), 5242, 2000.

Wang, J., et al., DS1 investigations of ion propulsion plasma environment: initial results, *J. Spacecr. Rockets*, subm., 2001.